



This is a repository copy of *On population-based structural health monitoring for bridges*.

White Rose Research Online URL for this paper:

<https://eprints.whiterose.ac.uk/185378/>

Version: Accepted Version

Article:

Gosliga, J., Hester, D., Worden, K. orcid.org/0000-0002-1035-238X et al. (1 more author) (2022) On population-based structural health monitoring for bridges. *Mechanical Systems and Signal Processing*, 173. 108919. ISSN 0888-3270

<https://doi.org/10.1016/j.ymssp.2022.108919>

© 2022 Published by Elsevier Ltd. This is an author produced version of a paper subsequently published in *Mechanical Systems and Signal Processing*. Uploaded in accordance with the publisher's self-archiving policy. Article available under the terms of the CC-BY-NC-ND licence (<https://creativecommons.org/licenses/by-nc-nd/4.0/>).

Reuse

This article is distributed under the terms of the Creative Commons Attribution-NonCommercial-NoDerivs (CC BY-NC-ND) licence. This licence only allows you to download this work and share it with others as long as you credit the authors, but you can't change the article in any way or use it commercially. More information and the full terms of the licence here: <https://creativecommons.org/licenses/>

Takedown

If you consider content in White Rose Research Online to be in breach of UK law, please notify us by emailing eprints@whiterose.ac.uk including the URL of the record and the reason for the withdrawal request.



eprints@whiterose.ac.uk
<https://eprints.whiterose.ac.uk/>

On Population-based structural health monitoring for bridges

J. Gosliga^{a,1}, D. Hester^b, K. Worden^a, A. Bunce^b

^a*Dynamics Research Group, Department of Mechanical Engineering
University of Sheffield, Mappin Street, Sheffield S1 3JD, UK*

^b*Civil Engineering, School of Natural and Built Environment, Queens University Belfast, Stranmillis
Road, Belfast, BT9 5AG, Northern Ireland*

Abstract

The maintenance and repair of bridges (and other large scale infrastructure projects) is a major area which could benefit from Structural Health Monitoring technology. Inspections on bridges can take a long time and require many people, and are therefore conducted infrequently. This low frequency of inspection leaves the chance that damage and dangerous critical failures can occur during the long timeframes between inspections. It might even be the case that an inspection fails to identify sub-surface damage. Therefore some form of continuous monitoring is desirable, especially if such systems can reliably detect sub-surface damage.

However, the application of SHM to bridges is made challenging by the cost and practicability of obtaining damage-state data for bridges. Over the lifetime of a single bridge, it is hoped that a critical failure will never occur, and only a small number of the possible damage states will occur. It is also unpractical to intentionally damage structures to obtain damage-state data.

Population-based structural health monitoring seeks to overcome the obstacle of the limited data available for a single structure, by allowing data to be shared between similar structures. Bridges represent an interesting challenge for PBSHM as each bridge is unique. As such, an assessment of how similar bridges are to each other is required. To provide this assessment, one must develop an abstract representation for each bridge, and using this to perform a comparison.

This paper describes the use of a general approach for assessing the similarity of structures, applied to several bridge examples which are representative of common types of bridges, to show that it can be applied in this field.

Keywords: Population-Based Structural Health Monitoring, Civil infrastructure, Bridge management systems, Data sharing

*Corresponding author - j.gosliga@sheffield.ac.uk

1. Introduction

2 1.1. Existing bridge management systems

There are a number of recent studies reporting on the deficits of existing infrastructure; for example, a backlog of bridge maintenance works in the UK - identified in 2019 - will cost £6.7bn [1]. Further, a French study showed that a third of 12000 state-maintained bridges across the country were in need of repair, and 840 were in danger of collapse [2]. In this context, managing bridges is a challenging task as there are many gradually ageing/deteriorating bridges, while the available maintenance budgets are in many cases constrained.

10 Currently, the bridges on a given network are managed via a system of periodic visual inspections undertaken by a bridge inspector. As part of this inspection, the different elements of the bridge are viewed and each element is assigned a condition score. Any damage present is noted and, where relevant, an appropriate repair is called for by the inspector. This information is then logged for each bridge on the network in a central database. Collectively, the system of inspections and the database are generally referred to as the bridge management system (BMS). The specifics of the BMS used varies between different countries/organisations [3]; however, the philosophy described above is common to them all. The BMS is then used by the bridge manager to identify top-priority maintenance, which in effect decides where the limited maintenance budget will be spent.

Unfortunately, not all bridge damage is readily identifiable via visual inspection, for example a railway bridge in Ireland [4] collapsed within days of an inspection, while a pedestrian bridge in Florida [5] collapsed only hours after an inspection. Therefore, the last two decades has seen a significant body of research into how much value sensor data could add to the existing management procedure. This work on the application of structural health monitoring (SHM) to bridges has seen many different approaches proposed, where the dynamic response of the bridge is analysed to identify the presence of damage. The proposed approaches tend to be either physics- based or data-based.

30 In broad terms, physics-based approaches exploit the underlying physics which govern the behaviour of the bridge to identify anomalous behaviour. For example, measuring acceleration [6, 7], displacement [8, 9], or rotation [10, 11]. Physics-based approaches notionally have the advantage that a given model is applicable to all bridges. However, the application of physics-based approaches are often limited by either (i) small subtleties in the dynamic response for each individual bridge (for example, a boundary condition that does not exactly match the theoretical ideal) or (ii) confounding influences, such as environmental conditions.

38 Data-based approaches [12, 13] do not rely on any physical understanding so they
are more robust to discrepancies between the model and the real world structure, or
40 variations arising from environmental conditions. However, data-based approaches
also have their limitations. Firstly, to implement supervised learning¹ requires a range
42 of normal condition and damage-state training data for that bridge. The necessary
damage-state data are practically never available as collecting such data would involve
44 allowing a real bridge structure to become (potentially critically) damaged. This issue
means that in the vast majority of cases the data models will employ unsupervised
46 learning, where the model is trained only on healthy-state data and subsequently looks
for anomalous behaviour.

48 In a situation where an operator is only concerned with one bridge, this is a reasonable
approach. However, if an operator were to have 1000 bridges, and 20 of these bridges
50 are very similar (for example, all constructed as part of the same road scheme), then
treating these 20 data models as entirely independent feels like a missed opportunity.
52 If these 20 bridges are genuinely similar in their design and construction, then the
dynamic behaviour of the bridges should be similar. Treating these 20 bridges as a
54 population (rather than individual structures) opens up the possibility of identifying
anomalous behaviour of a given bridge relative to the group. Work exploring how the
56 behaviour of an individual structure to that of a population was of similar structures for
the purposes of damage detection was carried out for a wind farm [14, 15]. Furthermore,
58 if at some point in the future, one of the 20 bridges experiences damage and data are
available for this event, these data can be used to improve the data models for all
60 bridges within the population.

This pooling of data would massively leverage the available information and hence is
62 a very attractive proposition. However, for it to be achievable it requires a systematic
way to measure ‘similarity’ between bridge structures, otherwise one can not define
64 the population of similar bridges. The next section describes such an approach where,
initially, structures are represented as graphs before the graphs are then compared to
66 calculate a similarity score.

1.2. Population-based structural health monitoring

68 The aim of Population-based structural health monitoring (PBSHM) is to increase
the availability of data and models for solving SHM problems, by sharing these
70 data between structures. In fact, if structures within a population of homogeneous
structures (structures that are nominally identical), a single model can be used to
72 describe the entire population [16]. However, to effectively transfer data and models
between structures that cannot be considered homogeneous, a certain level of similarity

¹Supervised learning describes a machine learning task, where a function is learnt that maps an input to an output based on example input-output pairs.

74 is required to avoid negative transfer [17]. Negative transfer occurs where classification
75 labels are inconsistent between the source and target domains; for example, either
76 each domain contains a different number of labels, or a pair of labels become switched.
This could be thought of in an SHM context as mislabelling the damage location,
78 type, or severity.

The question then becomes one of determining which structures are similar enough to
80 share models and data. This is a question that requires a quantifiable answer. A method
is therefore required for encoding qualitative information about the construction of
82 a structure so that a quantitative analysis of the similarity of two structures can be
performed.

84 The first step in the methodology applied here is to define the constituent parts of
the structure and describe them using *Irreducible Elements* (IEs). These Irreducible
86 Elements capture information about the geometry and material properties of each part
of the structure. Naturally, these elements feature physical connections between one
88 another, which are described by *joints*. Joints capture information about the physical
connection between two elements, such as whether the connection is fixed (*static*) or
90 free to move in some way (*dynamic*), as well as the location of the joint within the
structure. Together, the Irreducible Elements and joints form an Irreducible Element
92 model (IE model) [18] which describes the physical construction of the structure.

Once the IE model for a structure has been created, it will exist in a database. This
94 database will feature methods (functions) that allow for automatic comparisons to be
made between the various structures in the database. These comparisons are performed
96 by treating the information stored in the IE model as an attributed graph. By treating
the information as an attributed graph, existing graph comparison methods can be
98 used [19, 20, 21] to quantify the similarity between IE models.

The method for converting a structure into an IE model (and the subsequent conversion
100 of that IE model into a hypergraph for comparison purposes) is summarised in Section 2.

1.3. Contribution of this paper

102 In Section 1.1 the need for a new framework is described and Section 1.2 gives details
on the work on PBSHM to date. The focus of this paper is to extend PBSHM to
104 bridges and test whether meaningful comparisons can be made between real-world
structures. This is not a trivial exercise, as these real-world bridge structures are
106 much larger and have far more elements (e.g. by one or two orders of magnitude)
than the simple ‘toy’ structures that have been modelled to date. Hence, the current
108 work represents a significant validation of the PBSHM approach, testing whether this
approach can be applied across a population of real-world structures. It was also
110 important to test whether this approach generalised across different bridges. To that

112 end, five main bridge types (beam-and-slab, truss, cable-stayed, arch and suspension)
are included, which cover the vast majority of bridge constructions.

114 Including various bridge types also made it possible to check whether the similarity
scores between notionally similar bridges were sensible. To check this, an IE model
116 was developed for a second beam-and-slab bridge, a second truss bridge and a second
suspension bridge. The similarity scores between bridges of the same type were greater
118 than the similarity scores between dissimilar bridges, which is in line with what one
would expect based on engineering judgement. This the first time this approach has
120 been applied to real-world structures and represents a potential step change in how
bridges are managed.

The specific contributions of of the paper are:

- 122 • For the first time it is shown that PBSHM can credibly be applied to bridges,
covering all the major types of bridge construction
- 124 • The systematically calculated similarity scores returned by PBSHM are shown
to be sensible based on engineering judgement
- 126 • To accommodate some of the more complex bridge types, hypergraphs have
been used for the first time within the PBSHM framework

128 These contributions are delivered via the sections below. Specifically, Section 2
summarises existing work that has been carried on PBSHM. Section 3 describes the
130 bridges used in the study, the IE models prepared for each bridge and the resulting
graphs. The graph comparison method used is described in Section 4. The results
132 from the graph comparisons are given in Section 5.

The bridges studied in this paper are all real bridges. The beam and slab bridges
134 (Figures 6(b), 20(a) and 20(g)), the truss bridges (Figures 8(b), 20(b) and 20(h)) and
the tied-arch bridge (Figure 12(a)) are all on or over two lane highways in Northern
136 Ireland. The cable stayed footbridge (Figure 10(c)) is over a two-lane highway in
Exeter, UK. The two suspension bridges are recognisable as the Humber bridge
138 (Figure 14(a)) in the UK and the Bosphorus bridge (Figure 20(i)) in Turkey.

2. Background on population-based structural health monitoring

140 This section provides some background information on PBSHM; this section provides
only a brief overview of the process for creating IE models, since this process is
142 described in depth for bridges in Section 3. This procedure follows that laid out in [18],
with the main modification being the use of *hypergraphs* (described in Section 2.2.2),
144 as well as the use of attributes (described in Section 4). This section also provides the
graph definitions used in PBSHM that will be necessary for the rest of the paper.

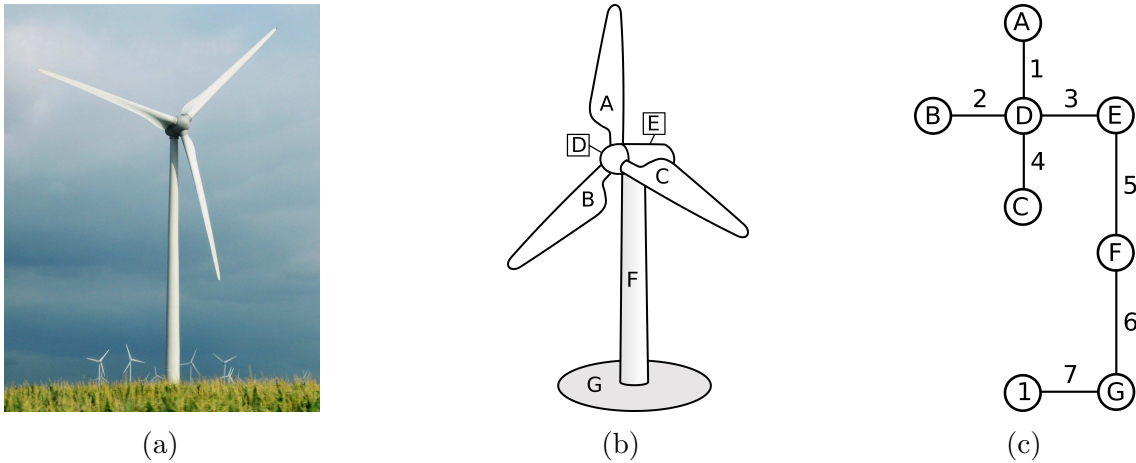


Figure 1: The evolution from a real structure (a) to an IE model (b) (with elements labelled) and finally into the attributed graph of the structure (c).

146 *2.1. Creating the Irreducible Element model for a structure*

To go from a real structure, such as the turbine shown in Figure 1(a) to an IE model,
 148 the first step is to break it down into structural elements called Irreducible Elements.
 These elements come with a description of their geometric properties and material
 150 properties, as well as a alphabetical label to identify the unique elements in the
 structure, shown in Figure 1(b). These elements possess properties which describe
 152 their materials and geometry, these element properties are illustrated in Table 1.

Table 1: List of elements and their properties for Turbine 1. FRP here stands for Fibre-Reinforced Polymer.

Wind Turbine					
Name	Element ID	Material Class	Material	Geometry	Shape
Rotor blade	A	Composite	FRP	Beam	Aerofoil
Rotor blade	B	Composite	FRP	Beam	Aerofoil
Rotor blade	C	Composite	FRP	Beam	Aerofoil
Rotor hub	D	Composite	FRP	Complex	Rotor hub
Nacelle	E	Composite	FRP	Shell	Cuboid
Tower	F	Metal	Steel	Beam	Cylindrical
Foundation	G	Ceramic	Concrete	Plate	Cylindrical
Name	Element ID	Boundary	-	-	-
Footing	1	Ground	-	-	-

154 The numbers outside of the circles in Figure 1(c) label the joints in the structure, which
 represent the physical connection between elements. These joints also possess properties
 which provide the location of the joints in the structure (as x, y, z coordinates), as

156 well as describing the nature of the connection between them; such joint properties
 are listed in Table 2.

Table 2: List of joints and their properties for Turbine 1

Wind Turbine						
Joint ID	Element set	Coordinate	Class	Type	Disp. DoF	Rot. DoF
1	{A, D}	(8, 15, 235.75)	Kinematic	Bearing	[x, y, z]	[y, z]
2	{B, D}	(8, 14, 254)	Kinematic	Bearing	[x, y, z]	[y, z]
3	{D, E}	(10, 15, 253)	Kinematic	Bearing	[x, y, z]	[y, z]
4	{D, C}	(8, 16, 254)	Kinematic	Bearing	[x, y, z]	[x, y]
5	{E, F}	(15, 15, 250)	Kinematic	Bearing	[x, y, z]	[x, y]
6	{F, G}	(15, 15, 5)	Static	Bolted	-	-
7	{G, 1}	(15, 15, 0)	Static	Clamped	-	-

158 Also shown in Figure 1(c) is the boundary condition element (denoted by the circle
 with ‘1’ inside) and corresponding joint (denoted by the joint label ‘7’) which shows
 160 where a boundary condition, such as the ground, interacts with the structure. The
 exact nature of the boundary condition is actually described by the joint between the
 162 boundary condition and the relevant element of the structure.

For a more detailed description of this method the reader should refer to [18].

164 2.2. Graphs and hypergraphs

2.2.1. Definitions

166 As well as graphs, hypergraphs can be used to describe these IE models, as described
 in brief here, along with the necessary graph and hypergraph definitions for the paper
 168 [22].

Definition 1: A graph G is defined by a pair $G = (X, E)$, where X is a set of
 170 elements and E is a set of edges. In a graph, each edge in E connects exactly two
 elements in X ; formally, $E \subseteq \{(x, y) | (x, y) \in X^2 \wedge x \neq y\}$.

172 **Definition 2:** A hypergraph is a generalisation of a graph where an edge can join any
 number of elements. Formally, a hypergraph H is a pair $H = (X, E)$, where X still
 174 represents a set of elements, but E now represents a set of subsets called hyperedges,
 $E \subseteq \mathcal{P}\{X\} \setminus \{\emptyset\}$, where \mathcal{P} is the power set.

176 **Definition 3:** A graph G' is said to be a subgraph of G , if $G' \subseteq G$, which implies
 $X' \subseteq X$ and $E' \subseteq E$, likewise, a hypergraph H' is said to be a subhypergraph H , if
 178 $H' \subseteq H$. Subgraphs (resp. subhypergraphs) are created by taking a subset of elements
 and hyperedges (resp. hyperedges) from the original graph (resp. hypergraph).

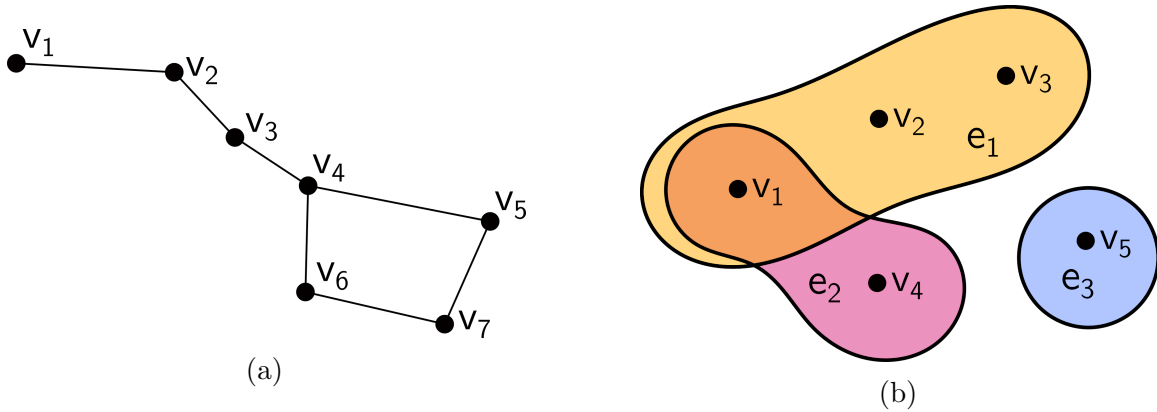


Figure 2: In a graph (a), each edge (solid black lines) connects exactly two elements (black circles). In a hypergraph (b), each hyperedge (shaded areas) connects any number of elements.

180 **Definition 4:** A subgraph (resp. subhypergraph) G' is said to be *induced* if for a
 182 subset of elements X' from G the edge set E' contains all edges from E that have
 both endpoints in X' , formally $E' = \{(x, y) \in E \mid x, y \in X'\}$.

Definition 5: The neighbourhood N of an element is the set of adjacent elements.
 184 For a graph, this is defined as $N(y) = \{x \in X \mid (x, y) \in E\}$.

Definition 6: A graph (resp. hypergraph) is said to be *connected* if there exists a
 186 path from any one element to all other elements in the graph (resp. hypergraph).

2.2.2. Use of graphs and hypergraphs in population-based structural health monitoring

188 Hypergraphs feature *hyperedges*, which can connect any number of elements (Def-
 inition 2); whereas, a graph features *edges*, which only ever connect two elements
 190 (Definition 1). As such, graphs are used to represent networks such as internet con-
 nections or social networks where each relationship is considered as only linking two
 192 elements. An example of a graph is shown in Figure 2(a). Hypergraphs, on the
 other hand, are used to represent data where a single relationship may link multiple
 194 elements, for example hyperlinks on a webpage or paper citations. An example of a
 hypergraph is shown in Figure 2(b).

196 Hypergraphs are useful for describing IE models, as there are certain cases where it is
 convenient to consider a single joint (edge) as connecting multiple elements. One such
 198 case is in truss structures, where multiple elements meet at either bolted or welded
 joints. A truss structure, as well as the resulting hypergraph, is shown in Figures 3(a)
 200 and 3(b) respectively.

It would also be possible to represent all the elements as being linked to only one other
 202 element to create a graph. However, this would create a more complicated graph, and

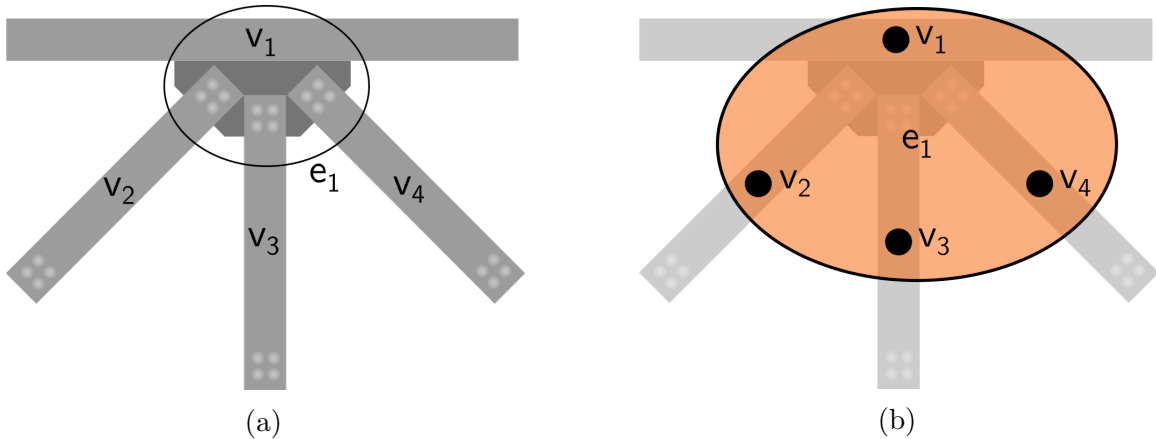


Figure 3: Panel (a) shows a truss structure with four elements (v_1, v_2, v_3, v_4) all meeting at the same point (e_1). Panel (b) shows the same truss structure, where e_1 is now represented as a hyperedge connecting all four elements of the truss structure.

may not be necessary to differentiate different structures. There is an argument that
 204 the web itself here could be considered as another element, thus creating a graph. In
 the final database implementation, it will be possible, where desired, to model every
 206 part of the structure using an element.

However, in structural analysis or truss structures, the web is not usually considered,
 208 and this is also typical in early stages of bridge design. By allowing multiple elements
 to be specified in an abstract hyperedge, flexibility is given to the user to reduce the
 210 detail in the IE model, where including such detail is not relevant to the comparison
 and would result in a more complicated IE model than is necessary.

212 *2.2.3. Visualising hypergraphs*

Hypergraphs can be visualised using different coloured areas to represent hyperedges;
 214 however, for more complex hypergraphs, this soon becomes unclear with multiple areas
 overlapping and elements becoming obscured. Hypergraphs can also be visualised
 216 using dummy vertices to represent the hyperedges, as shown in Figure 4. Again, with
 hundreds of elements and hyperedges, this would soon become incomprehensible.

218 One method that clearly shows the connections in the hypergraph, even when they
 become complex, is the Parallel Aggregated Ordered Hypergraph (PAOH) visualisation
 220 method [23]. In this method, the elements of the hypergraph are represented as rows
 and the hyperedges are represented as vertical lines with points where they connect
 222 to an element, as shown in Figure 5. The method was developed to visualise the
 evolution of 18th-century business relationships over time. This visualisation method
 224 is useful for bridges, as their IE models often result in complex hypergraphs that are

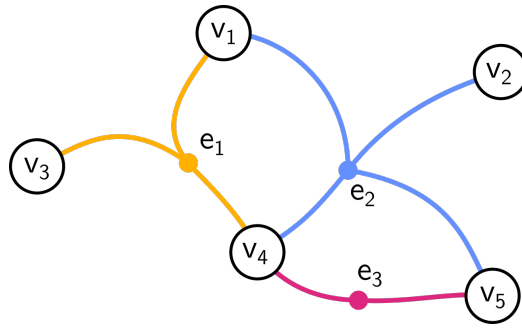


Figure 4: A hypergraph plotted using dummy vertices (e_1, e_2, e_3).

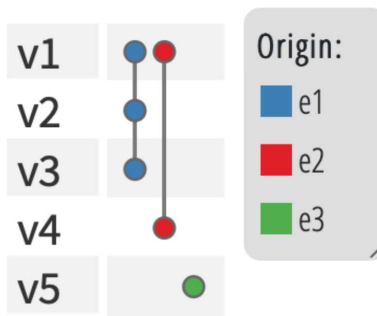


Figure 5: This figure represents the same hypergraph shown in Figure 2(b), but here the PAOH visualisation has been used, as generated using software on <http://www.di.uniba.it/~buono/paohvis/paoh.html>.

not easy to visualise using other methods, such as the dummy vertex or shaded area
 226 method.

3. Creating Irreducible Element models for five common bridge types

228 This section focuses on creating IE models for bridges of varying types, for the
 purpose of testing the ability of the attributed graph (or hypergraph) to represent
 230 different bridges and the ability of the chosen hypergraph comparison method to
 identify differences between them. Bridges can vary significantly in construction;
 232 therefore, a series of bridges are selected that can be categorised into five main types
 of construction. There could be arguments for more types of bridges to be defined;
 234 however, for the purpose of testing the application of PBSHM to bridges, the five
 categories are sufficient for capturing a range of bridge topologies. A summary of the
 236 five types are given in Table 3, and a description of preparing the IE models for them
 is provided in Sections 3.1 to 3.5.

Table 3: A table providing brief descriptions of the bridge types modelled in this study.

Bridge type	Description
Beam-and-Slab	These bridges are made up of two abutments (potentially with a number of intermediate piers). The deck is supported by longitudinal beams spanning between the supports. This is a very common type of bridge.
Truss	Variations within this type include the type of truss, the support conditions of the truss, and the location of the truss relative to the deck, e.g. the deck of truss bridges can be at the top, bottom, or middle of the truss.
Arch	An arch bridge is one where the deck is supported by one or more arches spanning between supports. The deck of an arch bridge tends to be either above the arch supported on struts, or below the arch supported on hangers.
Cable-Stayed	A cable-stayed bridge is one where the deck is supported by cables that connect directly to the pylon(s).
Suspension	Suspension bridges feature at least two towers with main cables running between them, anchored at abutments, with the bridge deck suspended from the main cables by hangers.

238 3.1. Beam-and-slab bridge

3.1.1. Beam-and-slab bridge description

240 The beam-and-slab bridge presented in this section is a real integral abutment beam-
 242 and-slab bridge in Northern Ireland. As an integral abutment bridge, the skeletal
 244 abutments are designed to flex with deck movement. A schematic of the elevation of
 246 the bridge and a photo of the bridge are shown in Figures 6(a) and 6(b) respectively.
 248 The vertical break lines in Figure 6(a) indicate the parts of the bridge that are shown
 250 in more detail in Figure 6(c), where a 3-D schematic of the bridge’s North abutment
 252 and intermediate pier are shown in the left and right of the figure, respectively. The
 254 South abutment is not shown, as it is merely a mirror image of the North abutment.
 256 The abutment and intermediate pier each comprise a foundation slab and four columns
 with a cap beam on top. In practice, the columns in the abutment are encased in
 concrete sleeves with an annulus of air between the interior of the concrete sleeve and
 the exterior of the column as is typical of integral bridge construction. However, for
 ease of visualisation the concrete sleeve is omitted from the diagram. The facing of
 the abutment evident on the left of Figure 6(b) is provided using a reinforced earth
 wall. The deck is formed using four precast concrete U-beams which sit on the cap
 beams, and are fixed in place by cast in-situ diaphragms. The diaphragms are cast at
 the same time as the deck slab, thus providing a fixed connection between the precast

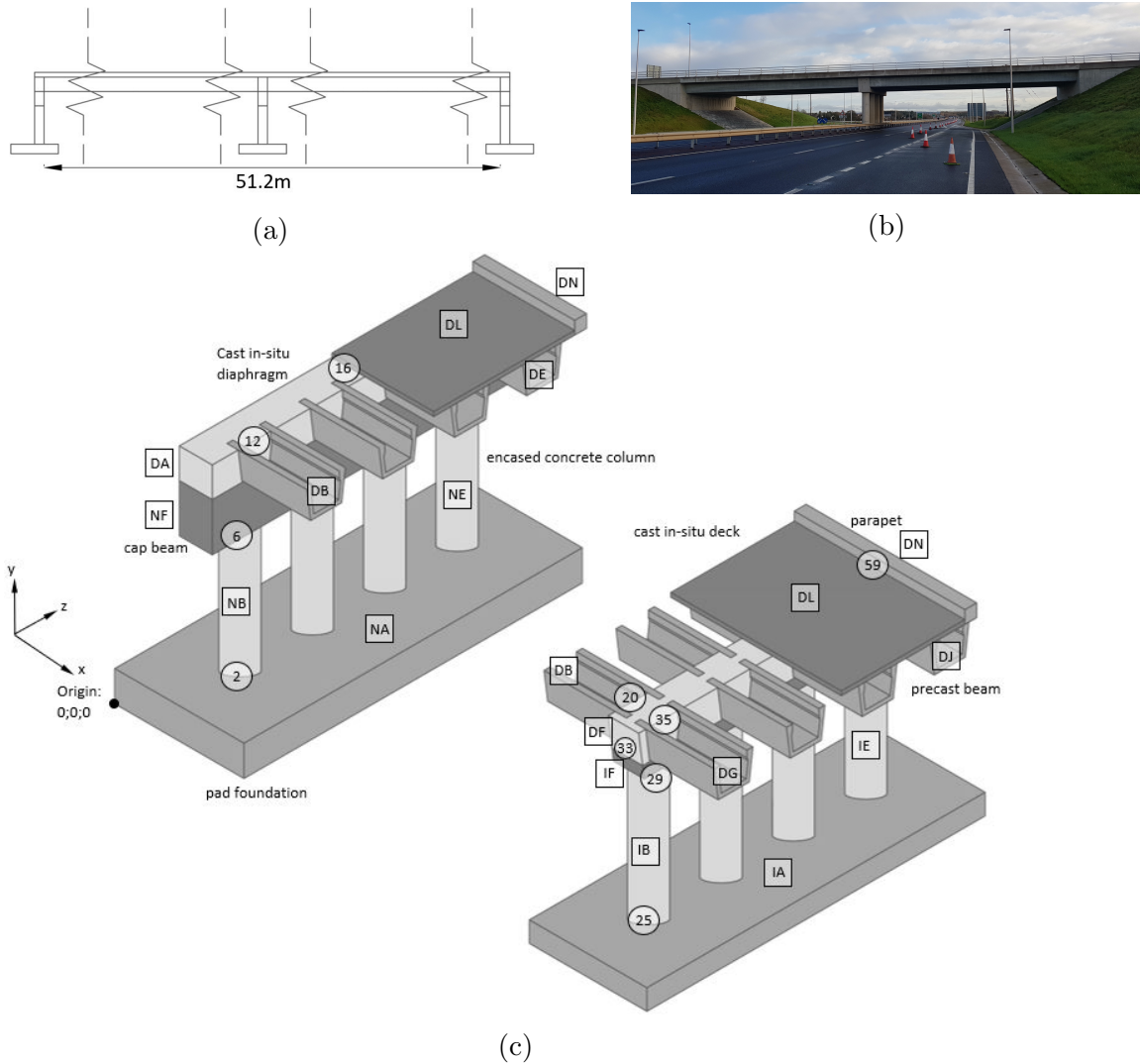


Figure 6: Beam-and-slab bridge: (a) schematic elevation of the bridge, (b) photo of the bridge and (c) stepped sections of the North abutment (left) and intermediate pier (right) annotated with Element and Joint IDs.

concrete U-beams of the deck, the deck slab, and cap beam. The element and joint labelling, square and circular markers respectively, are explained in the next section.

3.1.2. Beam-and-slab bridge: Irreducible Element model and Attributed Graph

Figure 6(c) shows the basic components of a beam-and-slab bridge. To convert this representation into an IE model, each element is first given a unique identifier. The Element IDs (letters) and Joint IDs (numbers) are shown in Figure 6(c) using square and circular markers, respectively. The rationale for the labelling shown is discussed later when presenting information in Table 5. However, before looking at the labelling

in detail, it is useful to understand that for each element defined with unique IDs, it is necessary to also capture the material class, material, element type and shape of the element. Table 4 presents some material classes, and the associated materials. The selection of the material class will dictate the range of materials that can be chosen from.

Table 4: Sample presets of information to choose from for Material Class and Material for each element.

Material class	Material
Metal	Steel
	Copper
	Aluminium
Composite	Reinforced concrete
	Prestressed concrete

The remaining properties to be defined for each of the elements are element type and shape. As this study is focussed on bridges, the classifications presented are relevant for bridges. It should be noted that, in the context of PBSHM, this list is not exhaustive as other other element types and shapes are necessary when describing other structures such as wind turbines or aeroplanes. The element types encountered for the set of bridges modelled include: beam, column, wall, slab, plate and cable. The corresponding shapes of the elements include cuboid, cylinder and trapezoid (solid and hollow), and C, I, T and U (precast beam shapes).

To demonstrate the IE modelling procedure, Table 5 shows a sample of each of the main elements of the beam-and-slab bridge deck bridge annotated in Figure 6(c). The table shows the initial information captured for each element. To avoid repetition, not all elements of the bridge are shown. The rows have been numbered R1-R11 to aid in referencing the table of elements (the information for the joints will be discussed later in Table 7). Table 6 presents the list of boundary conditions defined for the beam-and-slab bridge in Figure 6.

The left side of Figure 6(c) shows the North abutment of the bridge and the right-hand image shows the intermediate pier support. When describing the elements comprising these structures, the element IDs have been assigned the first letters ‘N’ and ‘I’ respectively. Elements pertaining to the deck have been given ‘D’ as the first letter. A naming convention of this sort for the Element IDs helps with the mapping of joints, particularly when a bridge has a large number of elements and becomes more complicated for joint mapping.

Starting on the bottom of the North abutment (see Figure 6(c)), the first element is the pad foundation. This element is labelled as NA, and is identified as having a material class, material, geometry class and shape shown in row R1 in Table 5. The next elements are the columns on the pad foundation, identified as NB to NE.

296 To avoid clutter in in Figure 6(c), the internal columns were not labelled, and to
 298 avoid repetition, row R2 only shows the properties for element NB but these are
 300 representative of each column’s attributes. The cap beam and diaphragm are labelled
 302 NF and DA, and their properties are defined in rows R3 and R4, respectively, of
 Table 5. The beam elements in the North span are labelled DB-DE, and the properties
 of DB are shown in row R5 (representative of the remaining beam elements also). The
 beams in the South span are labelled DG-DJ and the properties of DG are on row R6,
 also representative of the remaining South span beams.

304 The intermediate pier has a similar structure to the North abutment, with the same
 elements making up the support, but Element IDs prefixed with an ‘I’ in place of ‘N’.
 306 The captured information for the elements is shown in rows R9 to R11 in Table 5.
 The South abutment is a mirror image of the North abutment, but Element IDs are
 308 prefixed with ‘S’ in place of ‘N’. The South abutment is omitted from Figure 6(c) and
 Table 5 to avoid repetition.

310 The intermediate pier diaphragm is labelled as ‘DF’ in Figure 6(c) and has the same
 information as the North diaphragm ‘DA’ in row R4 of Table 5. The final elements of
 312 the bridge are the deck and parapet edge beams, with the deck labelled as DL and
 information presented in row R7. The element information for the Eastern parapet
 314 DM is shown in row R8, where the Western parapet would be identical but on the
 opposite side of the bridge.

316 Table 5 presents only a sample of elements to demonstrate how the element information
 is captured in the IE model. However, it is important to understand that in the
 318 IE model, each element has its own row, defined with additional information about
 the overall geometry for each element (length, breadth, depth), as well as material
 320 properties (Young’s Modulus, Poisson’s Ratio) that would be specific to that element.
 In total this bridge has 32 elements, and five boundary conditions – one for each
 322 support and two for each end of the deck.

Table 5: Element Table for elements shown in Figure 6(c), with additional column for Row number to aid discussion.

Row number	Description	Element ID	Material Class	Material	Geometry class	Shape
R1	Pad foundation	NA	Concrete	Reinforced concrete	Slab	Cuboid
R2	Column	NB	Concrete	Reinforced concrete	Column	Cylinder
R3	Cap beam	NF	Concrete	Reinforced concrete	Beam	Cuboid
R4	Diaphragm	DA	Concrete	Reinforced concrete	Beam	Cuboid
R5	Precast beam	DB	Concrete	Reinforced concrete	Beam	U
R6	Precast beam	DG	Concrete	Reinforced concrete	Beam	U
R7	Deck slab	DL	Concrete	Reinforced concrete	Slab	Cuboid
R8	Parapet	DM	Concrete	Reinforced concrete	Beam	Cuboid
R9	Pad foundation	IA	Concrete	Reinforced concrete	Slab	Cuboid
R10	Column	IB	Concrete	Reinforced concrete	Column	Cylinder
R11	Cap beam	IF	Concrete	Reinforced concrete	Beam	Cuboid

324 Once the elements of the bridge have been defined, and attribute information captured,
 the next stage is to define the boundaries of the structure (Table 6). The final stage

Table 6: Boundary Conditions of the first beam-and-slab bridge.

Element	Name	Boundary
Footing N	A	Ground
Footing I	B	Ground
Footing S	C	Ground

Table 7: Joints table for joints connecting members as annotated in Figure 6(c).

Joint ID	Element set	x-location	y-location	z-location	Type
1	NA, A	2.509331	20.349	6.2175	Soil
2	NA, NB	1.163573	21.849	1.593	Fixed
6	NB, NF	1.163573	25.924	1.593	Fixed
12	DA, DB	1.87143	29.049	1.62	Fixed
16	DB, DL	13.44143	30.0445	1.62	Fixed
20	DB, DF	25.01143	29.64	1.62	Fixed
24	IA, B	27.84933	20.477	6.2175	Soil
25	IA, IB	26.50357	21.477	1.593	Fixed
29	IB, IF	26.50357	28.29	1.593	Fixed
33	IF, DF	27.84933	28.865	6.2175	Fixed
35	DF, DG	28.01143	29.64	1.62	Fixed
59	DL, DN	30.98866	30.983	12.435	Fixed

is mapping the joints between the elements and, where relevant, boundaries of the structure (Table 7). The joints are numbered incrementally, and modelled as being at the centroid of where two elements meet. The location for the joint is defined using global X, Y and Z coordinates. The type of joint and its degrees of freedom are recorded, as well as the set of elements associated with the joint. A sample of the joints used in this model is provided in Table 7. As an integral-abutment bridge, each of the joints is identified as a fixed joint with no degrees of freedom associated (i.e. the joints are not designed to articulate), and as such, these columns have been omitted from Table 7.

Following the procedure outlined in Section 2.1, once the IE model has been fully described (using the approach shown in Tables 5 to 7), the next step is to convert the information into an attributed graph. No information is created or lost at this stage, it is simply rearranged to make it easier for the computer to perform comparisons between structures. The attributed graph (in this case) can be visually represented as either a simple graph as shown in Figure 7(a), or a hypergraph, as shown in Figure 7(b). The graph and hypergraph in Figure 7 are in fact identical; they have simply been visually represented in different ways.

Plotting structures as a simple graph, such as the one in Figure 7(a) has the advantage that the spatial and geometric significance (in relation to the real bridge structure) of

344 the graph topology is evident in a 2-D plot. The geometric significance of different
346 groupings of elements are annotated on Figure 7(a) to show how they correspond
348 to the actual bridge structure. However, visually representing the bridges as simple
graphs has the disadvantage that, as the number of elements increases, the groupings
become less evident.

To overcome this limitation, a hypergraph representation, such as the one shown in
350 Figure 7(b), can be used. Visually, the groupings are not as immediately evident in
the hypergraph representation as they are in the simple graph; however, by separating
352 out the elements and hyperedges, the information in the hypergraph representation
remains clear even with a large number of elements and joints.

354 The top row of Figure 7(b) concerns element DL, which is the deck slab (see Figure 6(c)).
Every hollow circle on this row represents a connection that element DL has to some
356 other element. Following the vertical lines dropping from these circles indicates which
other elements DL is connected to. In total on the first row there are 15 hollow circles
358 and this information is communicated as a summary bar chart down the left-hand
side of the figure. The second and third rows show the same information for elements
360 DF (diaphragm intermediate pier) and DA (diaphragm North abutment) respectively.
The remaining rows show the connections for the remaining elements. The numbers
362 (1-5) toward the bottom of the figure are the boundary conditions, so for example the
bottom row shows that boundary condition 3 is connected to element SA which is the
364 South abutment.

Due to the greater complexity of structures in the remainder of the paper, a hypergraph
366 representation will primarily be used. In addition, for later structures, occasionally
the joints will connect more than one element, which means they can no longer be
368 plotted as simple graphs.

3.2. *Truss bridge*

370 3.2.1. *Truss bridge description*

The first truss bridge modelled is a simply-supported, single-span footbridge located
372 in Northern Ireland and features a Warren type truss [24] for both walls of the bridge.
In general, truss bridges are more complicated and feature more elements than a
374 traditional beam-and-slab bridge, and multiple members may be considered as sharing
the same joint.

376 Figure 8(a) shows a schematic elevation of the bridge and Figure 8(b) shows a photo of
the bridge elevation. Figure 8(c) shows a 3-D view of a portion of the bridge, showing
378 the vertical plane of the truss as well as the horizontal members connecting the North
truss wall to the South truss wall. In this view it can be seen how several members
380 connect at the same point. The blue circled joint has been reproduced in Figure 8(d)
at a larger scale, to show a particular joint (59) that features six members connected

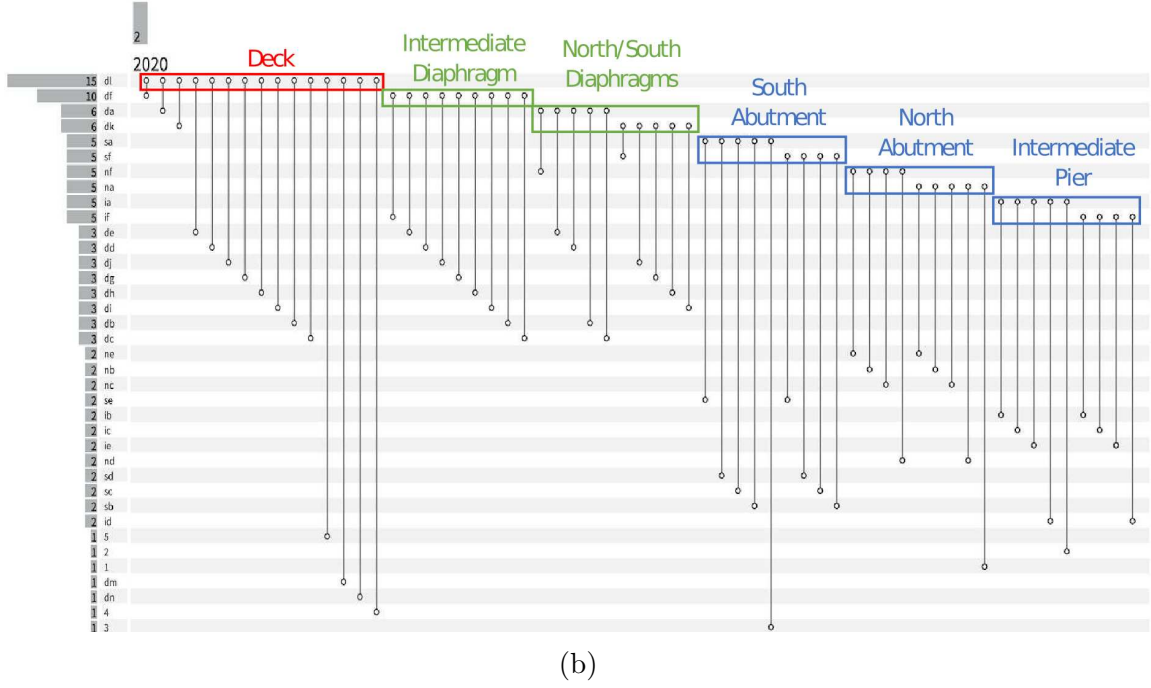
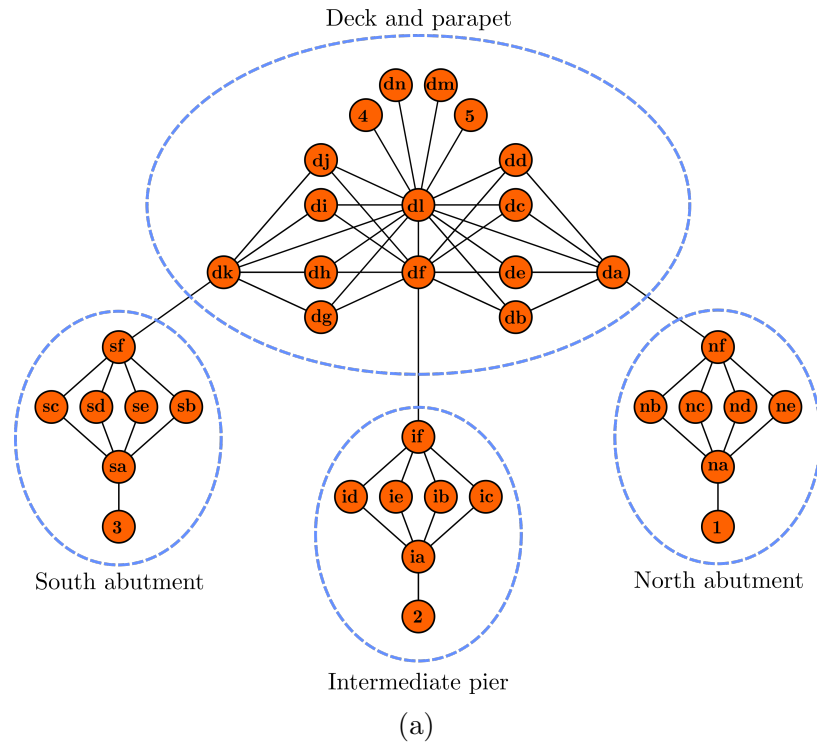


Figure 7: showing the attributed graph (a) where the elements in the attributed graph for the first beam-and-slab bridge have been labelled to show which sections of the bridge structure they correspond to, and (b) the same structure represented as a hypergraph.

Table 8: Element information for the truss bridge.

Description	Element ID	Material Class	Material	Geometry class	Shape
Top Chord South truss	SF	Metal	Steel	Beam	SHS
Inclined member South truss	SL	Metal	Steel	Beam	RHS
Inclined member South truss	SM	Metal	Steel	Beam	RHS
Transverse canopy member	CB	Metal	Steel	Beam	RHS
Bracing member in canopy	CJ	Metal	Steel	Beam	RHS
Bracing member in canopy	CK	Metal	Steel	Beam	RHS

Table 9: Example of a multi-element connection in the truss bridge.

Joint ID	Joint set	x-location	y-location	z-location	Type
59	SF, SL, SM, CB, CJ, CK	6.1	26.6098371	2.5	Fixed

382 at the same location. The beam elements have been greyed out and replaced with red
 384 lines to represent the elements (running through the centroid of the sections), with the
 red dot representing the joint location, at the centroid of where the members intersect.

A naming convention similar to the one used for the beam-and-slab bridge in the
 386 previous section was used for this truss bridge. The bridge spans East to West,
 resulting in ‘E’ and ‘W’ labels for the supports, and ‘N’ and ‘S’ labels for the North
 388 and South truss walls which form the primary structure of the bridge. Deck members
 again have the label ‘D’. Members pertaining to the canopy are labelled with ‘C’ ,
 390 where canopy refers to the horizontal elements joining the two top chords of the two
 truss walls.

392 3.2.2. Truss bridge: Irreducible Element model and Attributed Hypergraph

The joint detailed in the top right of Figure 8(d) (Joint ID: 59) features a continuous
 394 top chord beam element (SF) connected to 2 of the truss wall members (SL and
 SM), as well as three of the canopy members, one lateral (CB) and two diagonal (CJ
 396 and CK). The information captured by the IE model is the same as in the previous
 section and this information is shown in Table 8 for the selection of elements shown
 398 in Figure 8(d). Table 9 shows the joint information for joint number 59. The main
 difference between the joints shown in Table 9 and the joints shown in Table 7 is
 400 that there are six elements meeting at a single point, where the beam-and-slab bridge
 only ever had two elements per joint. Having given examples of how to prepare the
 402 element table (Tables 5 and 8) and joint table (Tables 7 and 9) that make up the IE
 model, to avoid repetition these tables are not presented for the cable-stayed, arch
 404 and suspension bridges modelled in Sections 3.3 to 3.5 respectively. However, the
 procedure used is the same.

406 The hypergraph for the truss bridge is shown in Figure 9. Comparing the hypergraph
 representation for the truss bridge in Figure 9 to the hypergraph representation of
 408 the beam-and-slab bridge in Figure 7, the first observation is the number of rows

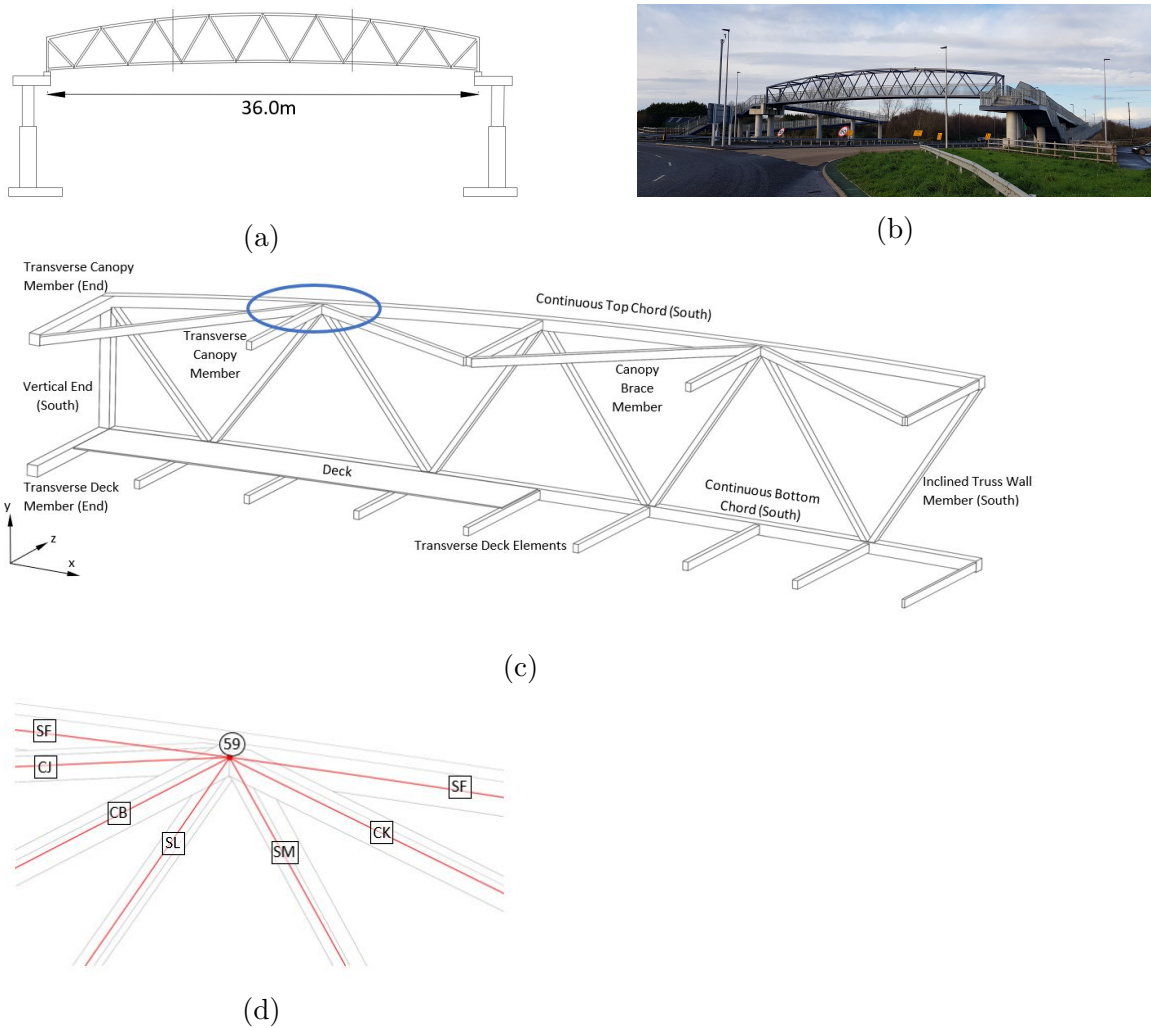


Figure 8: Truss footbridge: (a) elevation of bridge showing span, (b) photo of bridge elevation, (c) annotated stepped section of the bridge with top chord joint highlighted in blue and (d) zoomed and greyed out view of circled joint in (c) with element centroids drawn in red, joint location marked with red dot and element and joint IDs labelled (square and circle respectively)

in the table has increased from 37 to 109. This increase in rows is a result of the
 410 significantly greater number of elements required to describe the truss bridge. The
 412 second observation is that several of the vertical lines on the diagram intersect with
 multiple hollow circles. For example, the vertical line shown in grey relates to the
 elements shown in Figure 8(d), where the top hollow circle in the figure corresponds
 414 to element SF and, as one moves downwards, the circles correspond to elements CB,
 CK, and further down still, CJ, SL and SM.

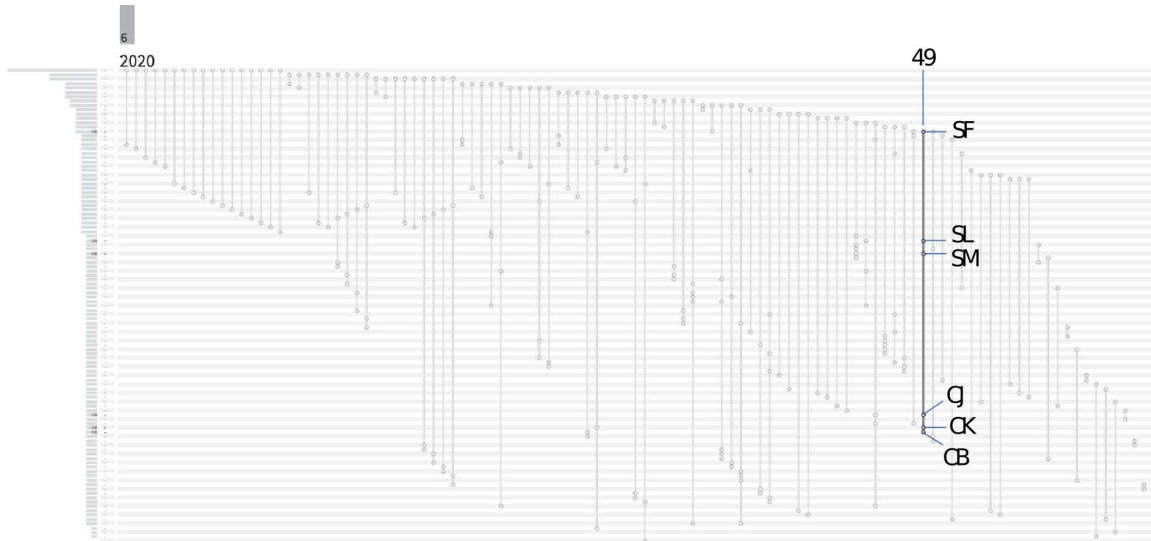


Figure 9: Hypergraph representation of the truss bridge, with the hyperedge corresponding to the joint described in Table 5 highlighted.

416 3.3. Cable-stayed bridge

3.3.1. Cable-stayed bridge description

418 The example cable-stayed bridge is a footbridge, shown in Figure 10, and located in
 Exeter, UK. Figures 10(a) and 10(b) show the elevation and end elevation, respectively,
 420 and Figure 10(c) shows a photo of the bridge. Figure 10(d) presents a stepped section
 of the bridge deck and it can be seen that cables attach to the deck via ‘transverse cable
 422 stay beams’ which run below the main longitudinal girders. The deck is supported on
 transverse beams which run between the longitudinal girders.

424 3.3.2. Cable-stayed bridge Attributed Hypergraph

The IE model for this bridge was prepared using the same approach as in Section 3.1.2,
 426 and the resulting hypergraph is presented in Figure 11. For ease of visualisation, the
 figure has some annotation along the top to indicate the different zones within the
 428 figure:

- The first row of the figure corresponds to the West longitudinal girder. As
 430 was shown in Figure 10(d), the East longitudinal girder is connected to many
 transverse beams and is also connected to a smaller number of transverse cable
 432 stay beams. Each of these connections is represented by the vertical lines
 dropping from the circles along the first row. At the bottom of each vertical line
 434 is a circle on the row corresponding to the element to which the longitudinal
 girder is connected. Collectively, this results in a triangular shape on the
 436 left-hand side of the figure.

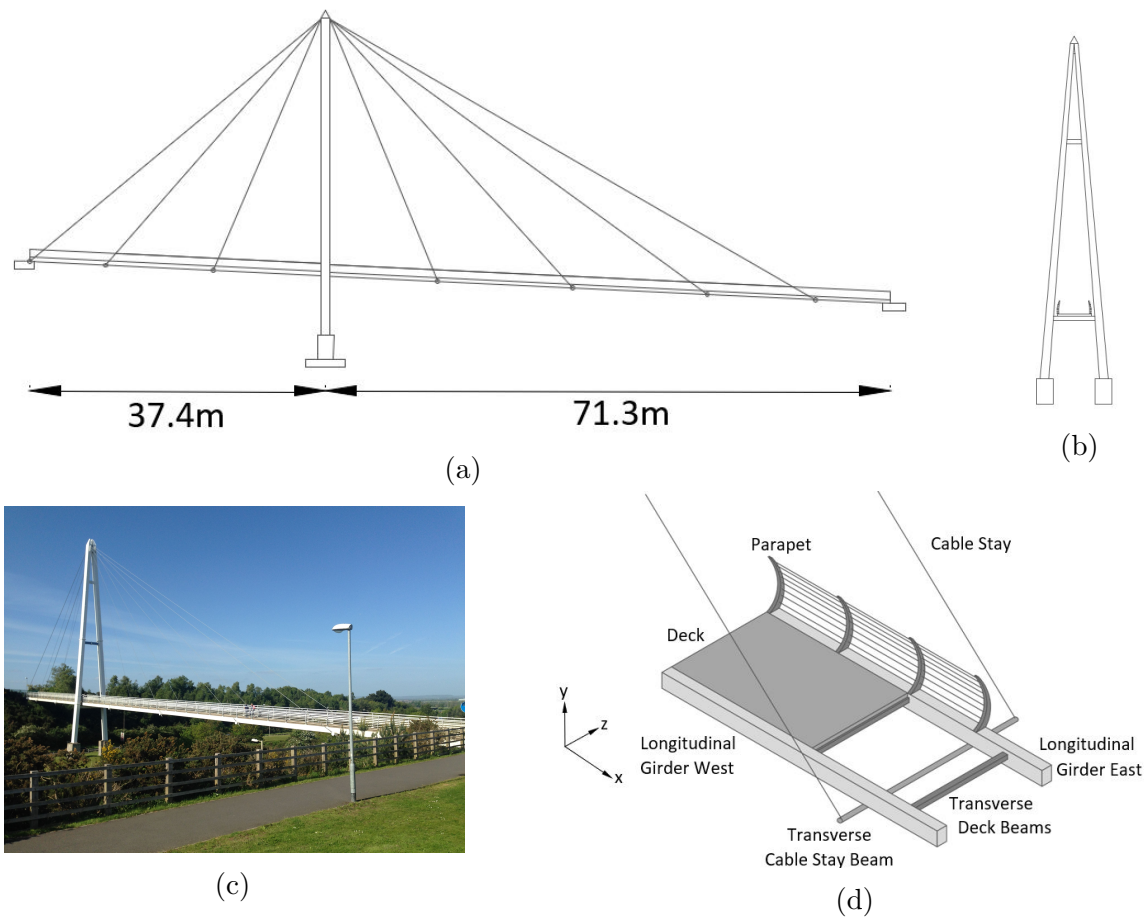


Figure 10: Cable-stayed footbridge: (a) elevation of the bridge, (b) end elevation (c) photo of the bridge and (d) part section of the deck with elements shaded and annotated.

- 438 • The second row of the figure corresponds to the West longitudinal girder and, as it is connected to the same elements as the East longitudinal girder, it results in an almost identical triangular shape.
- 440 • The third row of the figure represents the deck, which is also connected to the transverse beams so again a triangular shape results.
- 442 • The last portion of the graph, on the right-hand side, relates to the remaining elements of the bridge. In particular, the fourth and fifth rows of the hypergraph
- 444 represent the legs of the pylon.

A quick inspection of Figure 11 reveals that the bridge has relatively few multi-element
 446 joints, i.e. not many lines that have multiple circles on them. This bridge has 77
 448 elements, which is slightly fewer than the truss bridge described in the previous section,
 which had 109 elements.

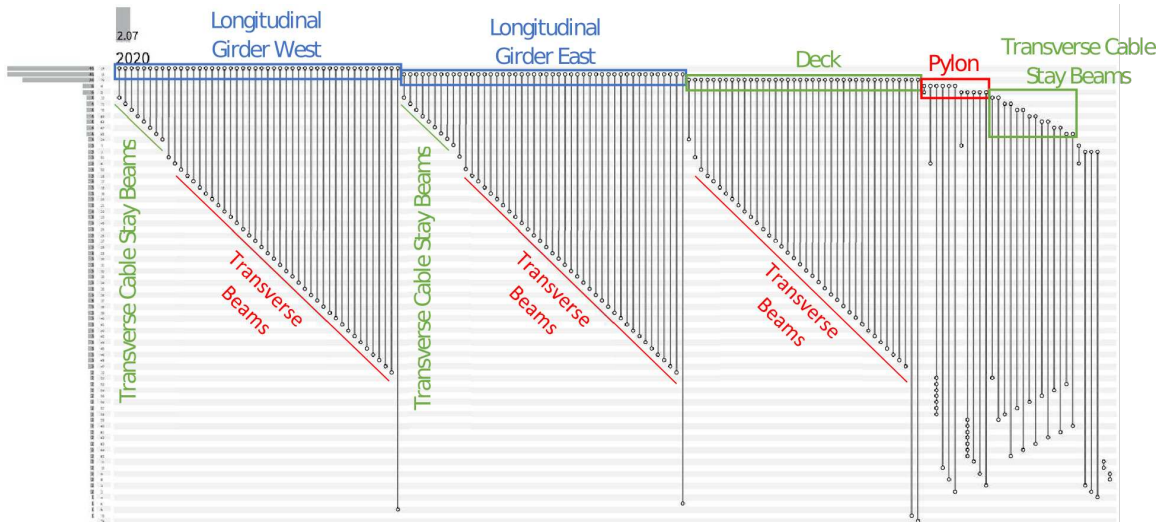


Figure 11: Hypergraph representation of the cable-stayed bridge.

The hypergraphs are plotted in such a way that the element with the most connections is plotted on the top row. This is referred to as the ‘degree of the element’ and this will be discussed further in Section 4.

3.4. Tied-arch bridge

3.4.1. Tied-arch bridge description

The arch bridge used in this study is an East/West-spanning 103m-span steel tied-arch bridge, located in Northern Ireland. The bridge features two independent box-section arches, one at each side of the bridge. Longitudinal girders tie the arches at each end of the bridge and provide vertical support from hangers coming from the arch. The deck is supported by transverse beams at discrete intervals along the length of the longitudinal girders. Figure 12(a) shows a photo of the bridge, Figure 12(b) shows a labelled schematic of part of the bridge, and Figure 12(c) shows an elevation of the bridge.

3.4.2. Tied-arch bridge Attributed Hypergraph

The IE model for this bridge was prepared using the same approach as in Section 3.1.2, and the resulting hypergraph is presented in Figure 13. Again, for ease of visualisation the figure has some annotation along the top to indicate the different zones within the figure.

The first two rows of the hypergraph represent the longitudinal girders which connect to both transverse beams and vertical hangers. The third row represents the deck, which connects to the transverse beams. The fourth and fifth rows represent the

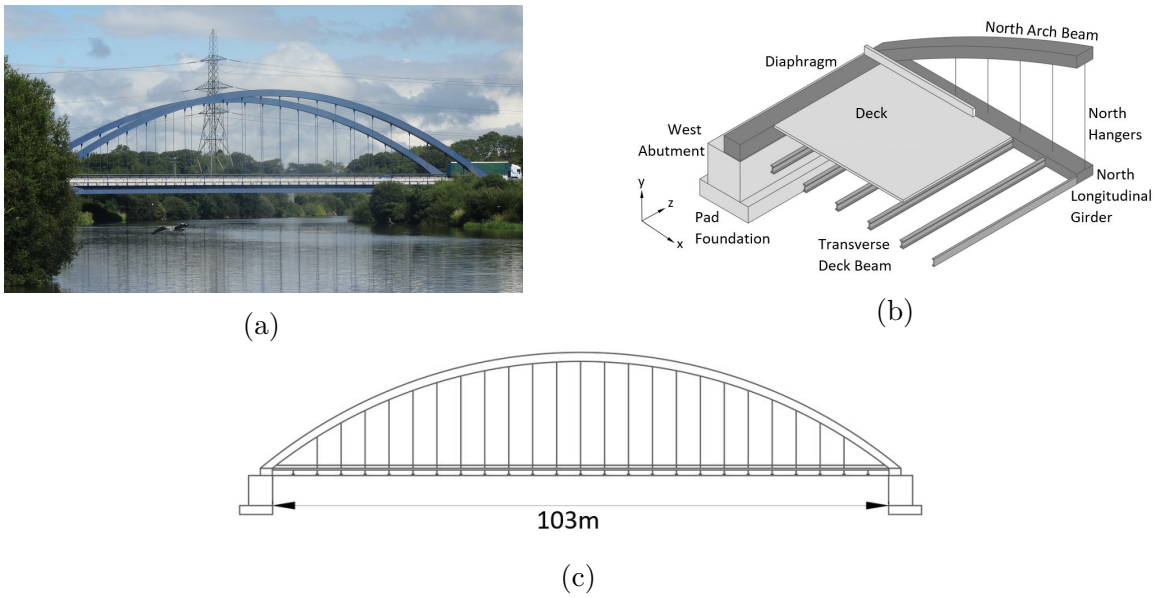


Figure 12: Tied-arch bridge (a) photo of the bridge, (b) shaded, stepped section of the bridge with labelled elements and (c) elevation of the bridge.

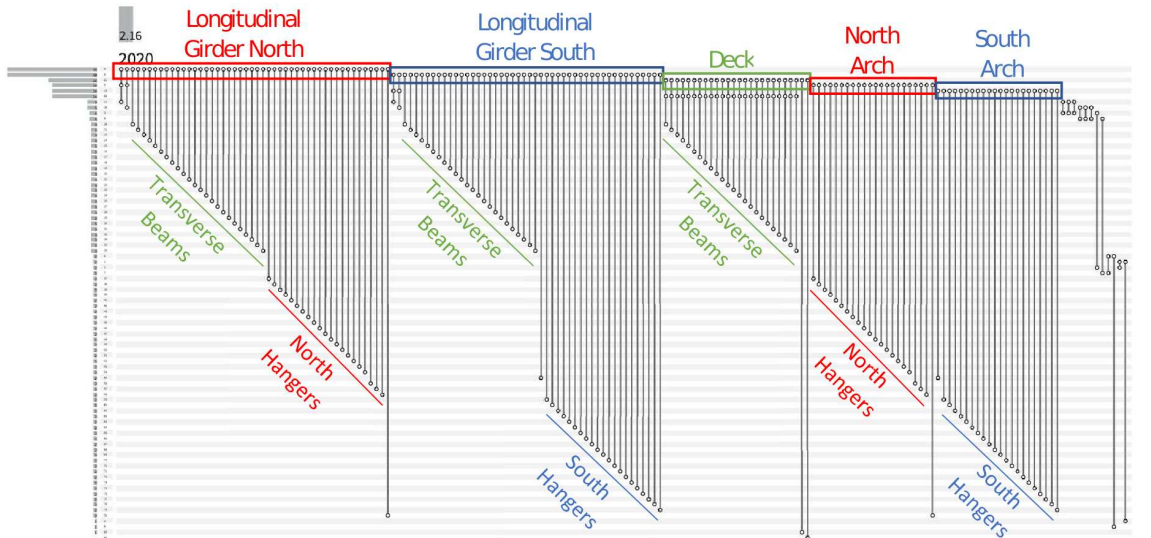


Figure 13: Hypergraph representation of the tied-arch bridge.

470 arches which are connected to the hangers. The remaining right-hand portion of the
graph relates to the bridge abutments.

472 The hypergraph in Figure 13 has a number of similarities to the graph for the cable-
stayed bridge shown in Figure 11; specifically:

- 474 • The ladder deck arrangement in both is leading to triangular patterns associated
with the longitudinal girders and the deck.
- 476 • Both bridges have relatively few multi-element joints, i.e. not many lines that
have multiple circles on them.
- 478 • Both bridges have a similar number of elements: 86 elements for the arch bridge,
compared to 77 for the cable-stayed bridge.

480 *3.5. Suspension bridge*

3.5.1. Suspension bridge description

482 The suspension bridge modelled for this study is the Humber suspension bridge (UK),
with a total span of 2.22km. The bridge comprises three spans of 280m, 1,410m, and
484 530m in a North-South direction. This bridge has a box-girder deck suspended from
main cables by an inclined-hanger system. The towers comprise a pair of tapered legs
486 and four cross beams, with foundations cast on hollow caissons. Figure 14(a) shows a
photo of the bridge, Figure 14(b) shows an elevation of a tower, Figure 14(c) presents
488 a section view of the North tower with element groups labelled, and Figure 14(d)
shows an elevation of the bridge.

490 *3.5.2. Suspension bridge Attributed Hypergraph*

The suspension bridge features by far the largest number of elements and joints of
492 any other bridge modelled in this paper, and as such, the hypergraph representation
is much larger than for previous bridges. Whilst dense, the hypergraph shown in
494 Figure 15 is still somewhat intuitive. The first row of the graph is the centre span of
the bridge deck. The second row is the main cable on the West side of the centre span,
496 and row three is the main cable on the East side of the centre span. The subsequent
three rows represent the South span, and rows 7 to 9, the North span.

498 As the deck connects to all hangers that also connect to the cables, the left-hand
shape that begins at row one is similar to the next two shapes, that begin from rows
500 two and three, combined. The fourth row is the deck for the South span and the fifth
row is the deck from the North span. The 6th and 7th rows are the main cables from
502 the South span and the 8th and 9th rows are the main cables from the North span,
with the same similarity again emerging between four, 6 and 7, as well as between
504 five, 8 and 9. The final portion of the graph, on the right-hand side, are the support

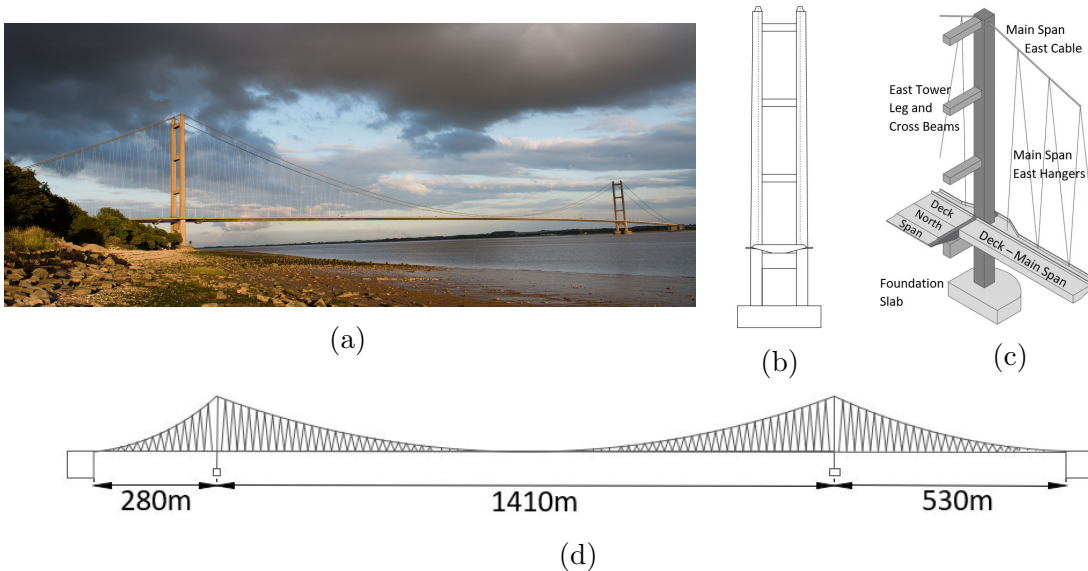


Figure 14: Suspension bridge, (a) photo of the bridge (b) bridge deck section showing elevation of the tower, (c) annotated stepped section of the north tower and (d) elevation of the bridge.

elements, such as towers and foundations. This was the largest graph produced so far, and tested the ability of the algorithm to cope with larger, more complex structures.

4. Graph comparison methods

4.1. Procedure for comparing two structures

Note: There is very little in this procedure specific to either graphs or hypergraphs. As such, to simplify the language in this section, the term ‘graph’ will be used to refer to both graphs and hypergraphs. Anything specifically relating to hypergraphs will be indicated as such.

Two bridges can be deemed similar if they share the same construction. To describe the construction of bridges it is useful to break them into elements. The structure (arrangement) of these elements and their material and geometric properties should provide a full description of the construction of the bridge. This gives a basis for determining similarity as if, for example, two beam-and-slab bridges share the same centre span construction, they should be considered more similar than any other bridges that feature a different design.

Therefore, the similarity scores described in this paper examine these two aspects of the bridges: the similarity of their structure, and the similarity of the materials and geometry within that structure. Two sets of elements will only be deemed identical if

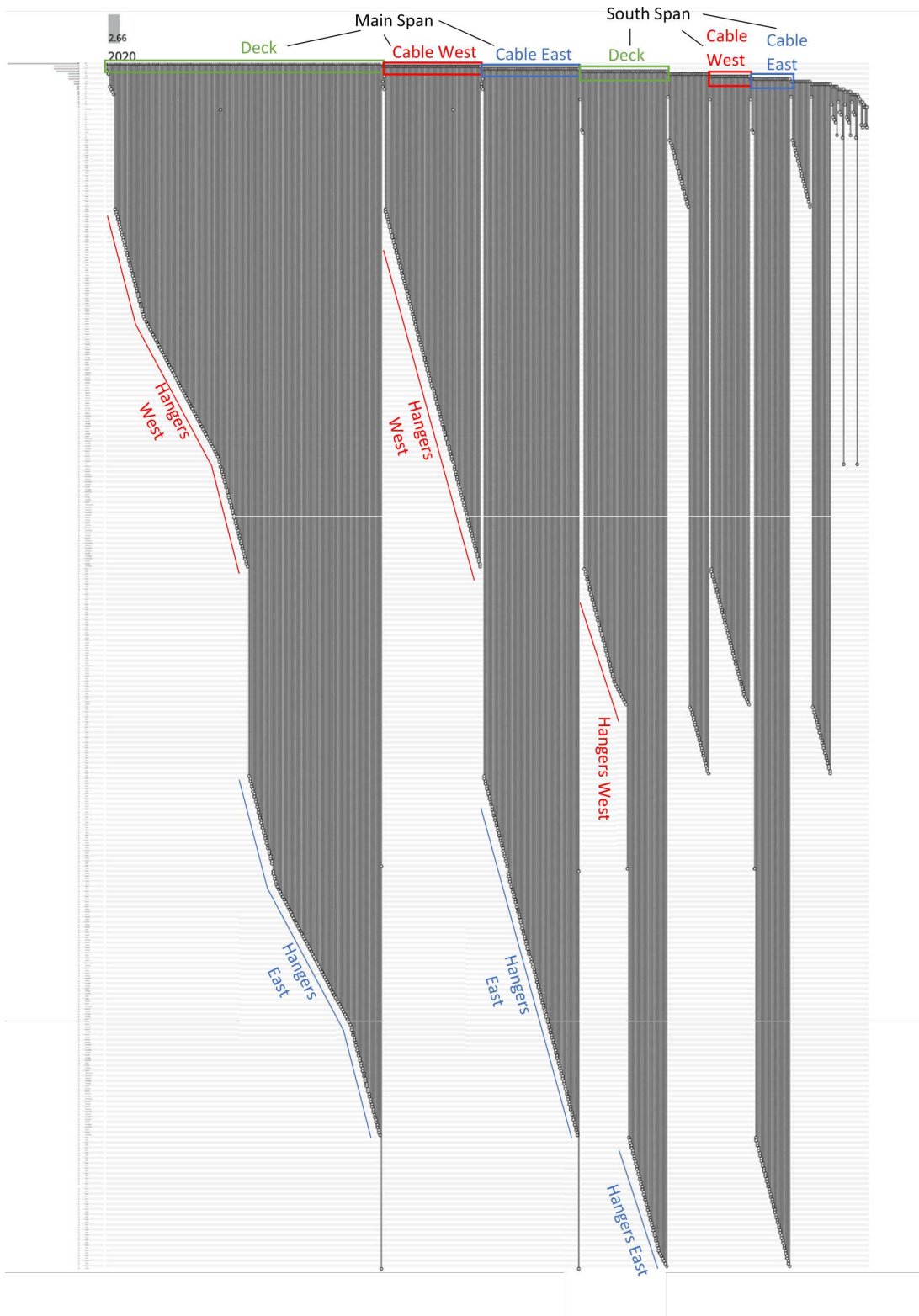


Figure 15: Hypergraph representation of the suspension bridge.

524 their structure is the same (they are arranged, i.e. connected, in the same way) and
their attributes (shape, geometry, material properties) are the same.

526 The set of elements that two bridges have in common represents the largest subcom-
ponent (subgraphs in the AG) they share, whether this be an entire truss structure
528 or simply a single pier of the same design that is common to both bridges. A large
set of elements that are common to both bridges would suggest that the two bridges
530 are similar. Two bridges that are completely different in design may only share the
deck as a common subcomponent, whereas if two bridges are identical, this common
532 subcomponent will be the entire bridge. The size of this subcomponent therefore gives
an indication of how similar the two structures are.

534 As mentioned, there are two ways in which two sets of elements can be similar. The
first way is if two sets of elements are connected in the same way, i.e. they have the
536 same topology. The second way is if all the attributes for the elements in one set (e.g.
shape or material properties, or both) are the same as the attributes of the elements
538 in the second set (referred to as attribute matching). Information about the topology
and attributes of a structure can be efficiently stored in the form of an attributed
540 graph. In this paper, both the topology and attributes of the graph will be checked to
determine the similarity of two bridges.

4.2. Description of graph-matching algorithm used

542 Graphs are used to describe the structure of the data, in this case the topology and
attributes included in the IE model, and facilitate comparisons between structures.
544 The graph for a structure can be further divided into subgraphs (Definition 3) for the
purposes of comparison.

546 Subgraphs describe subcomponents within the larger structures, for example, there
will be a section of the overall graph for a beam-and-slab bridge that describes a single
548 pier. Possible subgraphs between two structures are compared to see if they have
matching topology and attributes. This comparison is performed until the largest
550 subgraph (and hence subcomponent) between two structures has been found. The
largest subgraph between two graphs is known as the *maximum common subgraph*.

552 The process of finding the maximum common subgraph is referred to as graph-matching.
There are various methods for performing graph-matching. The method used in this
554 paper is an implementation of the algorithm described by [21]. This was chosen
over the classic Bron Kerbosch algorithm [19] and even the modified version [20] for
556 its superior computational speed and relative ease when it comes to implementing
attribute matching.

558 The algorithm described by [21], can be applied to two graphs G_1 , G_2 to find the
maximum common subgraph between them. The algorithm works by taking pairs of
560 elements (u_1, u_2) , where u_1 is an element from G_1 and u_2 is an element from G_2 . Each

of these pairs is checked to see whether or not they can form part of the trial solution.

562 The checks performed are as follows:

- 564 1. The attributes for u_1 and u_2 must match. This ensures that the properties of the elements (material, geometric) are the same. For this paper, only one attribute was used for each element.
- 566 2. Both u_1 and u_2 are adjacent to elements in at least one other pair that already forms part of the solution. This ensures that the resulting maximum common subgraph is connected – see Definition 6
- 568 3. The neighbourhoods (Definition 5) of u_1 and u_2 must contain the same number of matched elements. This ensures that nodes in the resulting maximum common subgraph are adjacent, if and only if they are adjacent in both parent graphs.
- 570 In simple graphs, this results in an induced subgraph – see Definition 4.
- 572

Figure 16 shows how the algorithm works. For the example shown in Figure 16, the attribute used for each element was the colour of the element. In the real bridge examples, the contextual labels were used as the attribute for each element. Contextual labels are attributes for an element that are purely human description, e.g. slab, beam, wall, column, that describe something of the function of that element within the structure.

The algorithm first selects 1b, as this element has the highest degree in G_1 , with a degree of 2. The pair (1b, 2b) is formed as 2b is one of the elements with the highest degree in G_2 . The other possible starting element would have been 1c as this also has degree 2, resulting in the initial pair (1c, 2b). This would lead to a different solution being reported, but in this case both these solutions would be equal in length.

584 Once the starting pair (1b, 2b) has been chosen, the first check is performed to see whether the attributes for the elements in this pair match. In this case, both elements have matching attributes (they are both white) so the pair is accepted. The second check does not apply at this stage since there are no pairs in the solution already, so it is not possible to check adjacency. The third stage is passed since the neighbourhoods for both elements in the pair contain zero matched elements. Therefore, this pair is accepted into the trial solution.

592 Using (1b, 2b) as the trial solution, the algorithm then moves on element 1c, since 1c has the highest degree out of the remaining elements in G_1 . (1c, 2a) is selected as 2a is one of the elements with the highest degree remaining in G_2 ². The attributes of 1c and 2a are then checked to see if they match. The attributes do not match, so this

²As with the first step, choosing 2c would lead to a different solution. The graph-matching algorithm will eventually explore all of these alternative choices and compare the resulting maximum common subgraphs to find the largest one. For simplicity, this backtracking procedure is not described here, but the interested reader can find the full procedure in [21].

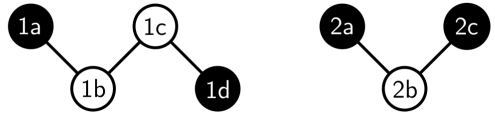
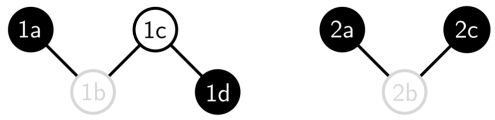
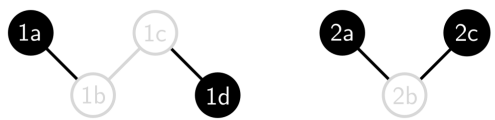
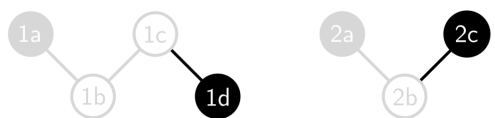

<p>1.</p> 	<p>Try: 1b - 2b : since this is the first pair to be tested, only the attribute check applies</p>
<p>2.</p> 	<p>Solution: 1b - 2b Try: 1c - 2a : fails attribute check 1c - 2c : fails attribute check</p>
<p>3.</p> 	<p>Solution: 1b - 2b Try: 1a - 2a : passes all checks</p>
<p>4.</p> 	<p>Solution: 1b - 2b 1a - 2a Try: 1d - 2c : passes attribute check, fails adjacency check</p>
<p>5.</p> 	<p>Solution : since there are 1b - 2b no more pairs 1a - 2a left to try, this solution is reported</p>

Figure 16: Illustration of the graph-matching algorithm. The colour of these elements can be considered as their attribute, with each element being either black or white. For G_1 , $X_1 = \{1a, 1b, 1c, 1d\}$ and $E_1 = \{(1a, 1b), (1b, 1c), (1c, 1d)\}$, and for G_2 , $X_2 = \{2a, 2b, 2c\}$ and $E_2 = \{(2a, 2b), (2b, 2c)\}$. The figure shows each iteration of the algorithm, starting with the initial solution (1b, 2b), checking every possible pair to see whether it can form part of the solution and eventually reporting the solution: (1b, 2b), (1a, 2a).

pair is excluded from the solution. Remaining on element 1c, the next pair to try is
596 (1c, 2c). Again, the attributes of these elements do not match so this pair is excluded
from the solution.

598 The algorithm now moves onto element 1a in G_1 . This then forms part of the pair
(1a, 2a). These elements have the same attributes. They are also adjacent to both
600 elements in a pair that already forms part of the solution, that is: 1a is adjacent to
1b and 2a is adjacent to 2b. These elements both have exactly the same number of
602 matched elements in their neighbourhood. This pair has passed all three checks and
can therefore be accepted into the trial solution.

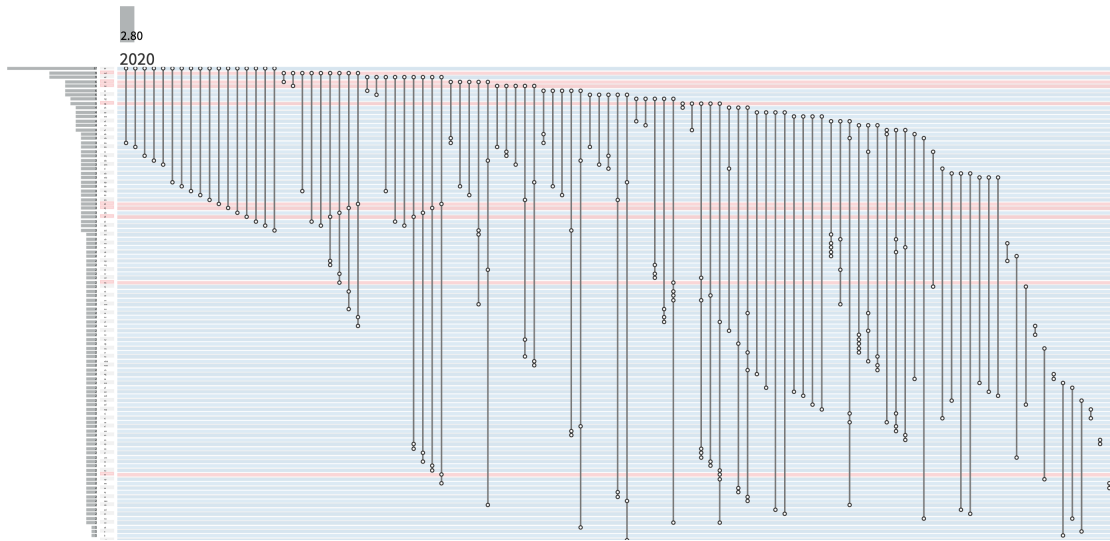
604 The algorithm now moves onto 1d in G_1 . This then forms part of the pair (1d, 2c)
since 2c is the only element remaining in G_2 that is not already in the solution. 1d
606 and 2c have matching attributes so this check is passed. However, while 2c is adjacent
to an element that forms part of the trial solution – 2b, 1d is not adjacent to any
608 element in the trial solution, and so the pair (1d, 2c) is excluded from the solution.
There are no remaining elements in G_2 that aren't already part of the solution and
610 can therefore be paired with 1d.

Since all of the elements in G_1 have now been visited, this particular search is considered
612 complete and the current trial solution is reported: (1b, 2b), (1a, 2a). If (1c, 2b)
had been chosen instead at the start, the reported solution would have been: (1c,
614 2b), (1d, 2c). These are both valid solutions for the problem of finding the maximum
common subgraph. Finding all valid solutions involves backtracking to previous steps
616 and trying the alternative combinations.

4.3. Graph-matching applied to the truss bridge and the beam-and-slab bridge

618 Applying the same procedure to the graphs for the truss bridge and the beam-and-slab
bridge, one arrives at the solution: (ND, DF), (NC, IF), (NE, DB), (NS, DC), (DF,
620 DD), (DJ, DE), (DL, DG), (SV, DK), and (SG, SF), where the first element in each
pair comes from the truss bridge, and the second element comes from the beam-and-
622 slab bridge. Figures 17(a) and 17(b) show a reproduction of the hypergraphs from
Section 3 for the truss bridge and beam-and-slab bridge, respectively, except this time
624 the elements for each that are included in the maximum common subgraph have been
highlighted.

626 In Figure 18, the maximum common subgraph is constructed using the elements for
each graph. Taking the first element in each pair of the maximum common subgraph
628 and taking the corresponding edges from the truss bridge graph gives the graph
shown in Figure 18(a). Taking the second element in each pair and including the
630 corresponding edges from the beam-and-slab bridge graph gives Figure 18(b). As
expected, both graphs in Figure 18 have identical topology.



(a)



(b)

Figure 17: PAOH visualisation for (a) the truss bridge and (b) the beam-and-slab bridge with the elements in the maximum common subgraph highlighted in red.

632 Since element pairs are only included in the maximum common subgraph if they
 633 have matching attributes, it can also be assumed that the corresponding elements in
 634 Figure 18 (ND and DF, DL and DG, etc.) have the same attributes. The conclusion
 635 is that the graphs shown in Figure 18 are in fact, identical. Therefore, the collection
 636 of elements that form the maximum common subgraph (shown in Figures 17 and 18)
 637 in each graph can be considered to have a similar construction. This collection of
 638 elements in fact gives the largest subcomponent shared by both bridges.

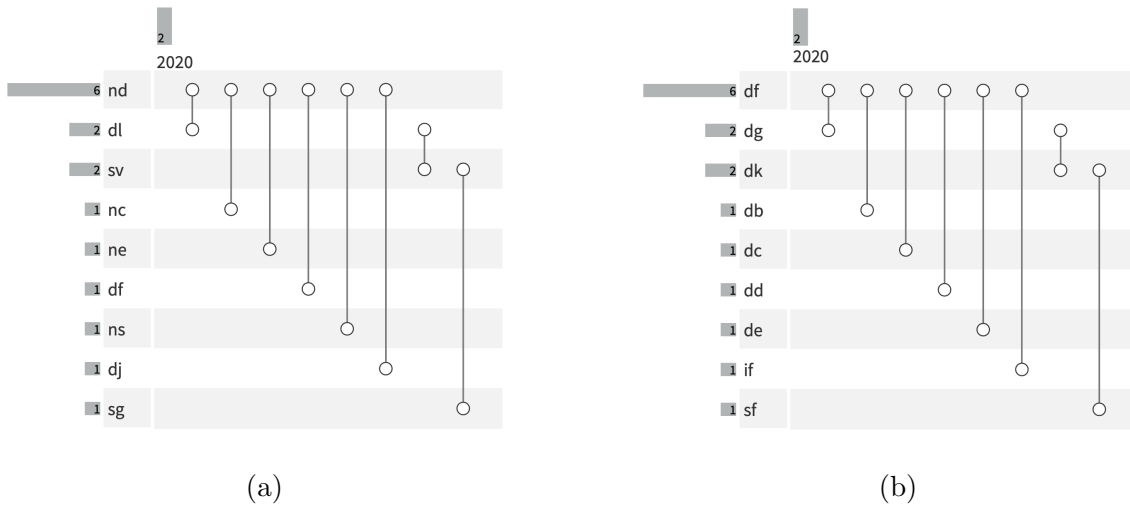


Figure 18: The structure of elements in the maximum common subgraph, where this structure is found in (a) the truss bridge and (b) the beam-and-slab bridge.

It should be noted, that due to the considerable differences in the construction of the two bridges, this subcomponent does not carry a large amount of physical significance. Examining the elements, one sees that this MCS is made up of interconnected beam elements in both bridges. The algorithm has aligned some of the beam elements in the truss with pre-cast and other beam elements supporting the deck in the beam-and-slab bridge. The elements in the truss bridge are: truss wall braces SV and NS; bottom chord elements NC, ND and NE; transverse deck elements DF, DJ and DL; and a top chord element SG. The elements in the beam-and-slab bridge are: precast beams DD, DE, DG, DB, and DC; cap beams IF and SF; and diaphragms DF and DK. It is clear that there is little structural significance in associating these sets of elements, and instead they were associated simply because they represent sets of beams with identical topology.

4.4. Repeating the graph comparison procedure for all five bridge types

The analysis in Section 4.3 shows the maximum common subgraph for the truss bridge and the beam-and-slab bridge; however, it is possible to apply this procedure to every possible pairing of the bridges described in Section 3, including comparing the bridges with themselves, which naturally returns a maximum common subgraph which is identical to the bridge itself. The size of the maximum common subgraph found for each of these bridge pairs is shown in Table 10.

Table 10: The number of elements in the maximum common subgraph for each pair of bridges. Note that where bridges have been compared with themselves, this number is simply the number of elements in that bridge’s hypergraph.

	Beam-and-slab	Truss	Cable-stayed	Arch	Suspension
Beam-and-slab	37	9	10	8	3
Truss	9	109	10	10	3
Cable-stayed	10	10	77	26	7
Arch	8	10	26	86	3
Suspension	3	3	7	3	476

658 *4.5. Calculating a similarity score based on the size of the maximum common subgraph*

660 For the purposes of demonstrating the graph comparison method, the Jaccard index will be used [25]. The Jaccard index was used because it is easy to implement and simple to understand.

662 This similarity index tells us how similar two sets of elements are, by comparing the intersection of the two sets with the union of the two sets. This is the number of
664 overlapping elements compared with the total number of distinct elements. This can be expressed mathematically as

$$J(A, B) = \frac{|A \cap B|}{|A \cup B|} = \frac{|A \cap B|}{|A| + |B| - |A \cap B|} \quad (1)$$

666 This means that the Jaccard index is essentially normalised with respect to the total number of elements and ranges between 1 and 0. If the similarity index is one, then
668 the two sets are the same. If the similarity index is 0, then the two sets are completely different.

670 In this case, the elements are the elements in the two parent graphs. The intersection is then the maximum common subgraph, as these can be considered shared between
672 the two graphs since they share the same attributes and topology. In the case of the truss footbridge and the beam-and-slab bridge, there are 109 elements in the truss
674 footbridge and 37 in the beam-and-slab bridge. There are 9 elements in the maximum common hypergraph between these two, so

$$J(A, B) = \frac{9}{109 + 37 - 9} = 0.066 \quad (2)$$

676 **5. Results**

Figure 19 shows the resulting similarity scores for the five bridges presented in Section 3.
678 The similarity scores in Figure 19 have been calculated using the method described



Figure 19: Shown are the resulting pairwise Jaccard similarity scores for the five bridges described in Section 3, calculated using the procedure described in Section 4. Cells which are green represent a close match between two bridges, while cells which are yellow indicate that two bridges are less similar.

in the previous section. The similarity scores between each bridge were calculated
 680 in the same fashion as for the truss footbridge and the beam-and-slab bridge, with
 the resulting similarity score of 0.066 shown (rounded to 0.07) in row 1, column 2 of
 682 Figure 19.

As can be seen from Figure 19, where bridges are compared to themselves, they are
 684 identical and (as described in Section 4.5) the similarity score is 1 and appears on
 the diagonal. It can also be seen that between most bridges the similarity scores are
 686 relatively low, and in most cases are 0.1 or less. The highest similarity occurs for the
 arch and the cable-stayed bridges. Here, both the arch and the cable-stayed bridge
 688 have a ladder deck construction, which gives rise to the higher similarity score. The
 least similar bridge was the suspension bridge, which is unsurprising as it is far more
 690 complex than the other bridges.

In conclusion, it was possible to describe all five different bridge types using IE models,
 692 and successfully convert these to graphs. Using the graphs, it was possible to compare
 all of the five different bridge types. The results of the pairwise comparisons for all
 694 five bridge types gave similarity scores which matched reasonably well with physical
 intuition, albeit that it is difficult to have a great feeling for the significance of the
 696 numbers.

The next step was to include bridges that would be considered similar to bridges that
 698 already existed within the population, and check if they returned scores that were
 consistent with what one would suspect based on engineering judgement.

700 *5.1. Revised table with extra bridges*

702 This sub-section investigates the introduction of three additional bridges to the existing
bridge population, assessing how the comparisons perform at identifying the similarities
704 between bridges of the same type. Section 5.1.1 describes the three comparator bridges
included, and Section 5.1.2 presents the results of the graph comparisons.

5.1.1. Comparator bridges used

706 Figures 20(a) to 20(c) show photos of the beam-and-slab, truss and suspension bridge
originally presented in Section 3. Figures 20(d) to 20(f) present some key structural
708 information about these bridges. Figures 20(g) to 20(i) show the three new comparator
bridges that have been introduced to the study. Figure 20(g) shows a beam and slab,
710 and Figure 20(h) shows a truss bridge, both located in Northern Ireland. Figure 20(i)
shows the Bosphorus bridge located in Istanbul, Turkey. Figures 20(j) to 20(l) present
712 some key information about the new bridges.

- 714 • For the beam-and-slab bridges, the key difference between them is that the
original bridge (Figures 20(a) and 20(d)) had skeletal abutments but the new
716 bridge (Figures 20(g) and 20(j)) has bank seat abutments. In essence, the deck
and intermediate pier of both bridges are quite similar, but the abutments are
718 significantly different. There are also some smaller differences, such as the bridge
in Figure 20(a) has four precast longitudinal beams per span, whereas the bridge
in Figure 20(g) has a slightly longer span and five precast beams per span.
- 720 • The two truss bridges are practically identical, with the main differences being
(1) the new bridge has a 2 m shorter span than the original bridge and (2)
722 the new bridge has piled foundations compared to the pad foundations of the
original.
- 724 • The new suspension bridge is similar to the originally-modelled bridge (Sec-
tion 3.5) in that it has a box girder deck and inclined hangers. However, the
726 main span of new bridge is appreciably shorter (1074m compared to 1410m) and
the back spans are supported on columns rather than being suspended from the
728 main cables via hangers like the centre span.

5.1.2. Results including comparator bridges

730 Figure 21 shows the results of including the three additional comparator bridges in
the analysis. The size of the maximum common subgraph found for each bridge pair
732 is shown in Table 11.

- 734 • The two beam-and-slab bridges show a similarity score of 0.51 (circled in red
in Figure 21). Intuitively, this feels a credible score as the middle portion of
both bridges is quite similar, but the ends are significantly different. Also, the

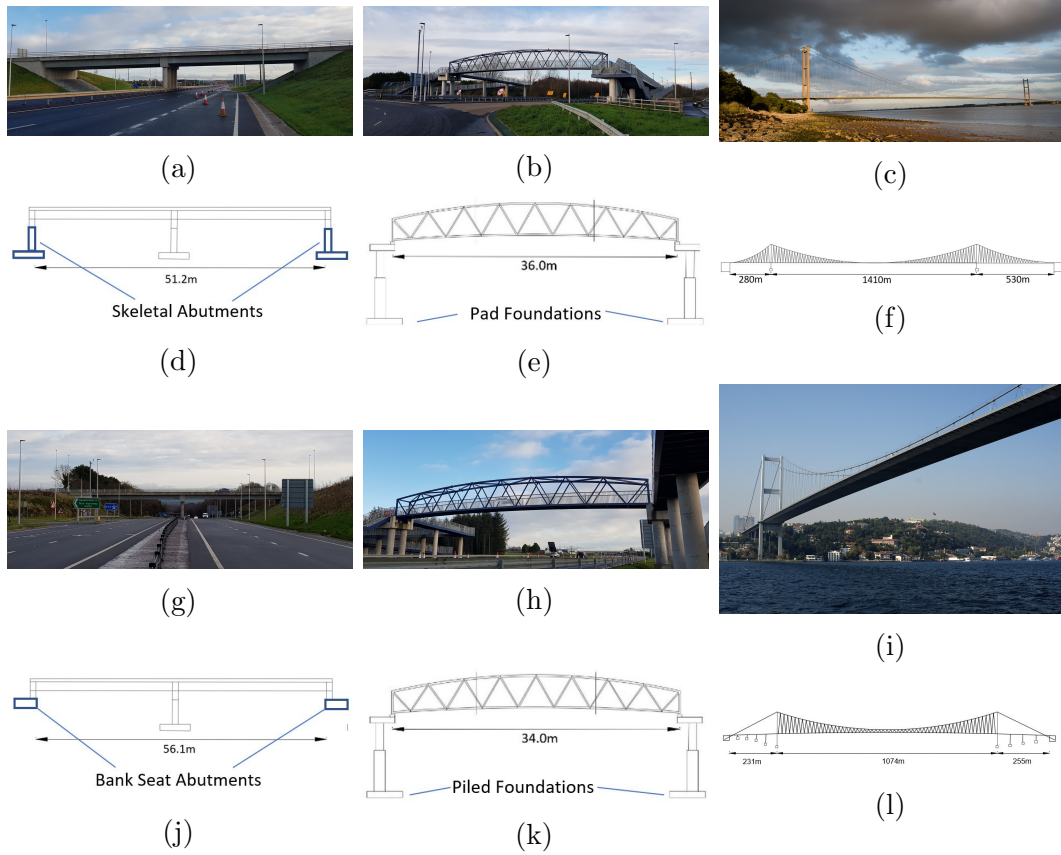


Figure 20: Three of the original bridges from Section 3 and the corresponding three comparator bridges (a) original beam-and-slab bridge, (b) original truss bridge, (c) original suspension bridge, (d) elevation of original beam-and-slab bridge, (e) elevation of original truss bridge, (f) elevation of original suspension bridge, (g) comparator beam-and-slab bridge, (h) comparator truss bridge, (i) comparator suspension bridge, (j) elevation of comparator beam-and-slab bridge, (k) elevation of comparator truss bridge, (l) elevation of comparator suspension bridge. Sub-figure (i) is titled “Boğaziçi Köprüsü / Bosphorus Bridge” by Jun Seita and is licensed under CC BY 2.0.

Table 11: The number of elements in the maximum common subgraph for each pair of bridges. Note that where bridges have been compared with themselves, this number is simply the number of elements in that bridge’s hypergraph. Some of the names of the bridges have been shortened to improve readability: beam-and-slab has been shortened to ‘B&S’, cable-stayed is now ‘Cable’, and suspension is now ‘Susp.’.

	B&S 1	Truss 1	Cable	Arch	Susp. 1	B&S 2	Truss 2	Susp. 2
B&S 1	37	9	10	8	3	23	10	7
Truss 1	9	109	10	10	3	10	107	3
Cable	10	10	77	26	7	12	10	3
Arch	8	10	26	86	3	8	10	3
Susp. 1	3	3	7	3	476	3	3	249
B&S 2	23	10	12	8	3	31	10	7
Truss 2	10	107	10	10	3	10	111	3
Susp. 2	7	3	3	3	249	7	3	304



Figure 21: Shown are the resulting pairwise Jaccard similarity scores for the five bridges described in Section 3 as well as the additional three comparator bridges described in Section 5.1.1, calculated using the procedure described in Section 4. Cells which are green represent a close match between two bridges, while cells which are yellow indicate that two bridges are less similar.

736 Beam-and-Slab 2 is slightly wider (five beams) than Beam-and-Slab 1 (four
 738 beams). The geometry of the elements and their materials was considered to be similar in this case.

- 740 • Truss 1 and Truss 2 have a similarity score of 0.95 (circled in black in creffig:results including comparator bridges). This high similarity score was expected, as these two bridges were deliberately selected to be very similar. The geometry of the members that make up the truss, as well as the materials used, were identical. 742 The only two differences between these bridges was that they were different sizes, and that one featured pile foundations. If a high score was not returned here, it would cast doubt on the validity of the approach. 744
- 746 • Suspension 1 and Suspension 2 have a similarity score of 0.47 (circled in blue in creffig:results including comparator bridges). Again this seems reasonable as the main spans of both bridges are quite similar, but the back spans are different. In 748 Figure 21, it is evident that the two suspension bridges show very low similarity to any bridge other than another suspension bridge. Considering the complexity of these two bridges relative to everything else, this is not surprising. 750

752 As the approach proposed here is new, it is difficult to have an exact feeling for the significance of the similarity scores. However, in broad terms, the magnitudes of the numbers discussed in the bullet points above appear to be consistent with what 754

one might anticipate based on engineering judgement, which is very encouraging.
756 Admittedly eight bridges is a small sample and hence significant further work is
required to be able to definitively prove the effectiveness of the approach.

758 **6. Conclusions**

This is the first time it is shown that PBSHM can credibly be applied to real-world
760 structures. This is done by creating IE models for five different bridge types which are
representative of the bridges that can be found in the real world. The general approach
762 to defining IE models was shown to be possible for bridges and can successfully capture
the different bridge types that one may find. The five bridge types examined were
764 beam-and-slab bridges, truss bridges, tied-arch bridges, cable-stayed bridges, and
suspension bridges. It was possible to describe all of these bridge types using the IE
766 model framework model developed for PBSHM.

Once these representations had been created for bridges, the systematically calculated
768 similarity scores returned by PBSHM are sensible/credible based on engineering
judgement. The graph-matching algorithm successfully grouped bridges that were
770 similar to one another. Beam-and-slab bridges were more similar to one another than
to the other bridge types. The truss bridges were more similar to one another than the
772 other bridge types. The suspension bridges were more similar to one another than the
other bridge types. The cable-stayed and arch bridge were found to be more similar
774 to one another, as they share a similar deck construction.

As mentioned in the introduction, this comparison of structures is necessary for
776 defining when data transfer is possible between structures. It is believed that it should
be possible to transfer data between bridges (or any other engineering structures) that
778 are grouped together by the graph-matching algorithm, and that where bridges are
not grouped, data transfer will be limited.

Another function of the graph-matching algorithm is finding the largest subcomponent
780 common to two structures. In two structures that are similar, this subcomponent is
likely to represent parts of the structure which exhibit similar behaviour, and therefore
782 if damage states occur within this subcomponent in one bridge, it should be possible
if damage states occur within this subcomponent in one bridge, it should be possible
784 to use this information to inform damage classification in the other.

This paper also introduces the use of attributed hypergraphs as a generalisation of
786 the attributed graphs featured in the other PBSHM literature. This paper briefly
introduces how hypergraphs can be used to describe structures and also why visualising
788 the data as hypergraphs is useful for complex structures such as bridges.

Acknowledgements

790 A number of the bridges presented in this paper are in Northern Ireland and hence we
would like to express our thanks to Northern Ireland Department for Infrastructure for
792 their support, particularly Daniel Healy and his team in HSU. The authors would like
to thank Graham Farrans Joint Venture, particularly Ross McWha, for their input
794 and information on common highway bridges. The authors would also like to thank
Devon County Council for their support in carrying out this work.

796 The authors would like to thank the UK EPSRC for funding through the Estab-
lished Career Fellowship EP/R003645/1 and the Programme Grant EP/R006768/1.
798 The authors would also like to thank the UK EPSRC for funding through grant
EP/R513118/1.

References

- [1] D. Browne. Cost of bridge maintenance backlog is £6.7bn. <https://www.transport-network.co.uk/Costof-bridge-maintenance-backlog-is-67bn/15557>, 2019.
- [2] R. Lobley. European bridge maintenance and safety. <https://www.governmenteuropa.eu/european-bridge-maintenance/92201/>, 2019.
- [3] H. Habeenzu, P.J. McGetrick, D. Hester, and S.E. Taylor. Bridge management systems- a review of the state of the art and recommendations for future practice. In *Proceedings of the Tenth International Conference on Bridge Maintenance, Safety and Management*, 2020.
- [4] Railway Accident Investigation Unit. *Malahide Viaduct Collapse on the Dublin to Belfast Line, on the 21st August 2009*, page 115. Railway Safety Commission, 2010.
- [5] A. Mohammad. *Investigation of March 15, 2018 Pedestrian Bridge Collapse at Florida International University, Miami, FL*, page 115. U.S Department of Labor, Occupational Safety and Health Administration, Directorate of Construction, 2019.
- [6] D. Hester and A. González. A wavelet-based damage detection algorithm based on bridge acceleration response to a vehicle. *Mechanical Systems and Signal Processing*, 28, 2012.
- [7] A. González and D. Hester. An investigation into the acceleration response of a damaged beam-type structure to a moving force. *Journal of Sound and Vibration*, 332(13), 2013.
- [8] D. Lydon, S.E. Taylor, M. Lydon, J. Martinez del Rincon, and D. Hester. Development and testing of a composite system for bridge health monitoring utilising computer vision and deep learning. *Smart Structures and Systems*, 24(6), 2019.
- [9] T. Khuc and F. Necati Catbas. Structural identification using computer vision-based bridge health monitoring. *Journal of Structural Engineering*, 144(2), 2018.
- [10] F. Huseynov, C. Kim, E.J. O’Brien, J.M.W. Brownjohn, D. Hester, and K.C. Chang. Bridge damage detection using rotation measurements – experimental validation. *Mechanical Systems and Signal Processing*, 135, 2020.
- [11] D. Hester, J.W.W. Brownjohn, F. Huseynov, E.J. O’Brien, A. Gonzalez, and M. Casero. Identifying damage in a bridge by analysing rotation response to a moving load. *Structure and Infrastructure Engineering*, 16(7), 2020.

- 834 [12] M. Döhler, F. Hille, L. Mevel, and W. Rücker. Structural health monitoring with
836 statistical methods during progressive damage test of S101 bridge. *Engineering
Structures*, 69, 2014.
- [13] B. Peeters and G. de Roeck. One-year monitoring of the Z24-bridge: environmental
838 effects versus damage events. *Earthquake Engineering and Structural Dynamics*,
30, 2001.
- 840 [14] I. Antoniadou, N. Dervilis, E. Papatheou, A.E. Maguire, and K. Worden. As-
842 pects of structural health and condition monitoring of offshore wind turbines.
*Philosophical Transactions of the Royal Society A: Mathematical, Physical and
Engineering Sciences*, 373, 2015.
- 844 [15] E. Papatheou, N. Dervilis, A.E. Maguire, I. Antoniadou, and K. Worden. A
846 performance monitoring approach for the novel Lillgrund offshore wind farm.
IEEE Transactions on Industrial Electronics, 62:6636–6644, 2015.
- [16] L.A. Bull, P.A. Gardner, J. Gosliga, T.J. Rogers, N. Dervilis, E.J. Cross, E.
848 Papatheou, A.E. Maguire, C. Campos, and K. Worden. Foundations of population-
based SHM, Part I: Homogeneous populations and forms. *Mechanical Systems
850 and Signal Processing*, 2020.
- [17] P.A. Gardner, L.A. Bull, J. Gosliga, N. Dervilis, and K. Worden. Foundations
852 of population-based SHM, Part III: Heterogeneous populations – transfer and
mapping. *Mechanical Systems and Signal Processing*, 2020.
- 854 [18] J. Gosliga, P.A. Gardner, L.A. Bull, N. Dervilis, and K. Worden. Foundations of
856 population-based SHM, Part II: Heterogeneous populations – graphs, networks,
and communities. *Mechanical Systems and Signal Processing*, 2020.
- [19] C. Bron and J. Kerbosch. Algorithm 457: finding all cliques of an undirected
858 graph. *Communications of the ACM*, 16:575–577, 1973.
- [20] I. Koch. Enumerating all connected maximal common subgraphs in two graphs.
860 *Theoretical Computer Science*, 250:1–30, 2001.
- 862 [21] Y. Cao, T. Jiang, and T. Girke. A maximum common substructure-based
algorithm for searching and predicting drug-like compounds. *Intelligent Systems
for Molecular Biology*, 24, 2008.
- 864 [22] R. Diestel. *Graph Theory, 3rd ed.* Springer-Verlag, New York, 2006.
- [23] P. Valdivia, P. Buono, C. Plaisant, N. Dufournaud, and J.D. Fekete. Analyzing
866 dynamic hypergraphs with parallel aggregated ordered hypergraph visualization.
IEEE Transactions on Visualization and Computer Graphics, 27, 2021.

- 868 [24] W. Lin and T. Yoda. Chapter Eight - Truss Bridges. In *Bridge Engineering*,
pages 137–153. Butterworth-Heinemann, 2017.
- 870 [25] P. Jaccard. Etude comparative de la distribution florale dans une portion des
872 alpes et des jura. *Bulletin del la Societe Vaudoise des Sciences Naturelles*, 37,
1901.